

# Curing dark energy instability with parametrized post-Friedmann treatment

Martín G. Richarte\*

*Departamento de Física, Facultad de Ciencias Exactas y Naturales,  
Universidad de Buenos Aires and IFIBA, CONICET,  
Ciudad Universitaria 1428, Pabellón I, Buenos Aires, Argentina*

Lixin Xu†

*Institute of Theoretical Physics, School of Physics and Optoelectronic Technology,  
Dalian University of Technology, Dalian, 116024, People's Republic of China and  
State Key Laboratory of Theoretical Physics, Institute of Theoretical Physics,  
Chinese Academy of Sciences, Beijing 100190, People's Republic of China*

(Dated: June 15, 2022)

We review the parametrized post-Friedmann (PPF) method within the framework of interacting dark energy model for a FRW background. We assess the possibility of using such treatment for curing a “bad” interaction from its large-scale instabilities, usually presented within the standard linear perturbation theory. Regarding the Markov Chain Monte-Carlo analysis, our global fitting combines several cosmological probes including the cosmic microwave background (WMAP9+Planck) data, barion acoustic oscillation (BAO) measurements, JLA sample of supernovae, Hubble constant (HST), and redshift-space distortions (RSD) measurements through the  $f\sigma_8(z)$  data points. The joint observational analysis of Planck + WP + JLA + BAO + HST + RSD data leads to a coupling parameter,  $\xi_c = 0.00140^{+0.00079}_{-0.00080}$  at  $1\sigma$  level for vanishing momentum transfer potential, whereas the aforesaid value is reduced in a 0.022% when the momentum transfer potential is switched on. The CMB power spectrum shows up a correlation between the coupling parameter  $\xi_c$  and the position of acoustic peaks or their amplitudes. The first peak's height increases when  $\xi_c$  takes larger values and its position is shifted. We obtain that the relative difference, in the CMB power spectrum, between the vanilla model and our best-fit cosmology remains below 0.2% in module.

PACS numbers: draft

## I. INTRODUCTION

Our current view of the Universe is based on the large amounts of observational data coming from the measurements of cosmic microwave background anisotropies (CMB) from different surveys, for example, the well known WMAP9 project [1] and the European satellite called Planck [2], [3], [4]. More precisely, the statistical analysis performed with the Planck polarisation spectra at high multipoles  $\ell > 50$  shows a good agreement with the best-fit  $\Lambda$ CDM cosmological model [4], composed of a constant dark energy density plus cold dark matter, while some tension could appear in the low multipoles zone ( $\ell < 40$ ), confirming previous finding obtained by WMAP9 team [1]. In order to improve the former analysis, galaxy surveys such as 2dFGRS [5], SDSS [6], 6dFGS [8], [9], and VIPERS [13] turn to be extremely useful because can be used as complementary tools for analyzing the large-scale structure of the Universe; which involves the exploration of the clustering properties of many sample of galaxies, the growth rate of cosmic structures or how redshift-space distortions in clusters could lead to better cosmic constraints [14], [15], [16], [17], [18], [19], [20], [21], [22] along with possible detection of barion

acoustic oscillation (BAO) signal in the power spectra of galaxies [23], [24], [25], [26]. Another reliable source of cosmic information concerns to the photometric distance measurements at high redshift of type Ia supernovae [27], [28]; in fact, the multi-color light curves from these standard candles provided the first successful evidence employed for showing that the Universe is currently accelerating [29]. Nowadays, the supernovae surveys have increased the number of events trying to put further constraints on the nature of dark energy through the estimation of its equation of state [30], [31]. As a general picture, we can say that modern cosmology relies on the existence of two unknown components; a pressureless fluid responsible for clustering of galaxies (dark matter) and a mysterious fluid with enough negative pressure for driving our Universe toward an accelerating phase (dark energy). However, the evolution from an early era dominated by dark matter era and its transition towards a dark energy dominance at late times is not completely understood, mostly because such mechanism requires a full understanding of the physics behind the dark sector.

Despite the amazing observational evidences supporting the vanilla model, some fundamental questions regarding the true nature of dark energy remain elusive yet. In this context, one puzzle refers to the great disagreement between the theoretical value predicted for vacuum dark energy density and its observational bound [32]. Another pitfall of the concordance model is the so called coincidence scandal, namely dark energy does not vary

\*Electronic address: martin@df.uba.ar

†Electronic address: lxxu@dlut.edu.cn (corresponding-author)

but dark matter fades away as the Universe expands, so why the amount of dark energy and the fraction of dark matter could exhibit the same order of magnitude at present. Although this fact could be considered by some researchers as just pure causality without any deep physical meaning behind, its true relevance only can be judged once a microscopic theory for dark energy is found and therefore is confronted with the observational data. At this point, the first issue usually is addressed by considering a dynamical dark energy approach where the speeding up of the Universe is driven by an homogenous scalar field dubbed quintessence field [33]. In order to alleviate the coincidence problem, a novel mechanism proposes to include some exchange of energy between dark energy (quintessence field) and dark matter components [34], [36]. This scheme was extended to the case where dark energy is accommodated as a general fluid [37], [38]. A quite remarkable fact about coupled quintessence or general interacting dark energy model is the possibility of having scaling solutions (attractor) for describing the late stage of the Universe. In particular, coupled quintessence models with scaling solution were analyzed by several authors [39], [40], [41], [42], [43], [44]. The stability of scaling solution also was examined by including cosmological perturbations of the background [45], [46].

Once an interaction between the dark components is selected, the next step is to confront its related background dynamic as much as it is possible with all the recent observations. The dynamic of galaxies within a cluster seems to be a nice place where starts to seeking a new kind of signature or constraint about the parameter space spanned by the dimensionless coupling [47], [48], [49]. Coupled quintessence models have been faced observational data in diverse scenarios and the large scale-structure of the Universe is one of them [50], [51], [52], [53]. The luminous rotation curves for spiral galaxies and the dynamical properties of galaxies were both used to put further constraints on the parameter space spanned by coupling function [48]. In addition, it was suggested that coupled dark energy model leads to a novel mechanism for accelerating the infall velocities of the Bullet cluster [51]. Cosmic structure formation at the galaxy cluster scale seems to be affected by the existence of non-vanishing coupling in the dark sector [54], [55]. For instance the number of cold dark matter haloes (halo abundance) predicted is compatible with the recent detections of massive high redshift galaxy clusters [54]. Mildly constraints on the coupling parameter for coupled quintessence model are obtained when the integrated Sachs-Wolfe (ISW) effect at late time is included through the analysis of the low multipoles zone in the CMB power spectrum [56]. These studies are considerably improved when the global statistical analysis includes different data sets such as Planck, BAO, the compilation of supernovae Ia called Union 2.1, and CMB lensing data [57]. In this context other kinds of constraints can be found by studying the evolution equation of the growth factor [58] or combining Planck+HST sets

for tightening the dimensionless coupling parameter [59].

A second approach requires to leave aside the coupled quintessence models and proposes an ad hoc interaction in terms of general cosmic fluids. The exchange of energy could lead to a distinctive evolution of the background equations or perturbation equations [60], leaving some imprints on the Universe. This would allow us to constrain a particular type of interaction using the recent observational data released by Planck combined with supernovae and BAO data among other probes [61]. It should be mentioned that in most of the cases, the recent data are considerably enough for determining the present value of the dimensionless coupling with a good accuracy [61]. Some analysis focus on the role played by the interaction in galaxy clusters [62] or use the redshift-space distortion data for obtaining better constraints on the interaction coupling [63]. As is expected the transfer of energy between dark matter and dark energy could also affect the standard behavior of dark energy at the recombination epoch by avoiding that its amount fades away too quickly [64]. Hence, the observational data would detect such singular feature and therefore will put some stringent constraints on the fraction of dark energy at early times [65], [66], in fact, updated bounds are now available after Planck data were released [4].

The framework of linear perturbation theory in its diverse versions [67], [68], [69], [70], [71] allows us to examine in detail whether an instability can occur or not for interacting dark energy models. Further, there is a public code dubbed CAMB developed by Lewis *et al.* which can be used for testing the stability of perturbed cosmological system [72] and finding the best-fit value of cosmological parameters, including the interaction coupling, by means of a Markov Chain Monte Carlo statistical approach (MCMC) [73]. The possibility of having an instability in the interacting dark sector depends on several facts but mostly on the specific of the interaction vector. The first example of instability appeared in the literature in the case of coupled scalar field model based on Chameleon-like theory [74], [75]. In those works, the exponential growth of small perturbations took place in the adiabatic regime on small scale because the squared sound of speed becomes negative for time-scale smaller than the Hubble time defined as  $H^{-1}$ . Later on, it was found that the adiabatic sound speed can remain considerably small implying the growth of linear density perturbations are small, so the perturbations become stable indeed [76]. The role played by instabilities when matter is coupled to scalar field was also analyzed in [77], indicating that the exchange of energy breaks down the adiabaticity condition provided the relative entropy perturbation and its derivative can not set both to zero initially. On the other hand, non-adiabatic instability gives rise on the early radiation era for the interacting dark sector when the exchange of energy is proportional to dark matter density regardless of the small values taken by its dimensionless coupling parameter; the aforesaid fact was discovered in [78] and re-analyzed in [79], [80]. It was

noted that the appearance of an instability in the perturbation equations can be traced through the effect introduced by an extra-term (doom factor) which is proportional to the interaction function and appears involved in the dark energy pressure perturbation [79]. When the interaction is proportional to dark energy density the instability fades away if the dimensionless coupling parameter is small enough, as a matter of fact, the allowed values of coupling parameter are intrinsically related to how close the dark energy equation of state is of the phantom divide line  $-1$  [80]. Subsequently, the relation between the adiabatic initial conditions and the existence of instability in the dark sector was analyzed more carefully in [81] while the observational impact of these interactions were analyzed in series of articles [82], [83]. Other forms of exchange of energy were proposed to avoid the so called non-adiabatic instabilities in the dark sector [84], [85], [86]. It should be stressed that the interaction form applied in [86] for avoiding large-scale instability was also proposed in [87] for evaluating the relationship between unified model, like Chaplygin gas, and interacting dark energy models.

One appealing manner to carry out the linear perturbation is employing the so called parametrized post-Friedmann (PPF) formalism designed by Hu and Sawicki several years ago [88], [89]. The PPF approach relies on the strong assumption that dark energy density perturbation must remain smaller than the dark matter perturbation [89]. This treatment introduces a new dynamical function called  $\Gamma$  along with its master equation. In doing so, the perturbation equations for dark energy density and its momentum are replaced and turned to be unified under this single function. In this sense, dark energy density fluctuations and its momentum become derived magnitudes, being obtained in a consistent way only through the evolution of  $\Gamma$ . The method becomes self-consistent provided the full perturbed Einstein equations along with the perturbed conservation equations (i.e. continuity and Navier Stokes balance equations) are satisfied for a Friedmann-Robertson-Walker (FRW) metric [88], [89]. In order to obtain a smooth interpolation between the large scale and small scale limits, it is mandatory to impose on superhorizon that the curvature perturbation (in the co-moving gauge) are conserved at second order in the wave number while in the opposite limit (quasistatic regime) the metric must fulfill a Poisson-like equation [89]. However, the study of near-horizon perturbation requires that the transition scale must be determined numerically [89]. The mentioned formalism has a wide spectrum of applicability because it can be used for testing a departure from GR as well [90], [91], [92]; as occurs with the PPN formalism where one seeks deviations from Newtonian's gravity. For example, it was employed for analyzing the crossing of phantom divide line with multiple scalar fields [91]. Regarding modified gravity theories, this approach was used for obtaining forecast constraints with the future Planck data on specific  $f(R)$  model [93] but also looking for new signatures

coming from galaxy clustering in the case of quintessence models or modified gravity model [94]. In fact, some authors elaborated brand-new and different PPF-like methods in a general consistent manner according to the modified gravity theory under study [95], [96], [97], [98], [99], [100], [101] and analyze their corresponding cosmological impact as well [102], [103], [104], [105].

The relationship between the pressure and density fluctuation for dark energy is not forced by hand, so the non-adiabatic instability related to dark energy perturbations might disappear in the PPF method. As a matter of fact, it was shown that after having applied the PPF treatment to the case of interacting dark energy model with an exchange of energy proportional to dark matter density, the perturbation equations do not exhibit the usual large-scale instability at early time [106]. For the latter reasons, our aim is to apply the PPF procedure to the same kind of "bad" interaction seeking to examine the persistence or not of such large-scale instability when the covariant form of momentum transfer potential changes, thus, we will consider not only the case with an interaction vector proportional to dark matter four velocity but also to dark energy velocity, generalizing previous results. In addition, we will constrain the  $c_T$  parameter of the PPF formalism under a global statistical analysis including different observational data such as "JLA" sample of supernovae [31] and the growth rate of cosmic structure [18], [19], [20].

The structure of the paper is as follows. In Sec. II, we first review the covariant treatment of linear perturbation theory, indicating all changes introduced by taking into account an explicit transfer of energy between dark matter and dark energy, some details are mentioned in the Appendix A and B. We devote Sec. III to mentioning all usual gauge choices, including the comoving gauge, while the synchronous gauge is mentioned in Appendix C. In Sec. IV, we illustrate how the PPF approach works in a very general manner, calculate the source term in the synchronous gauge also, and study the background evolution for a given interaction, determining the momentum transfer potential in two cases among other issues. In Sec. V, we perform a MCMC statistical analysis for determining the best-fit value of the cosmic parameters and compare them with the standard values reported by Planck and WMAP9 missions; we also explore the position and amplitude in the CMB power spectrum. Finally, the conclusions are stated. We refer to reader to Appendix D for the perturbed equation of dark matter variables in synchronous gauge.

## II. BACKGROUND AND PERTURBATION EQUATIONS

Let us assume an homogenous and isotropic Friedmann-Robertson-Walker spacetime for the back-

ground metric

$$ds^2 = a^2(-d\eta^2 + \gamma_{ij}dx^i dx^j), \quad (1)$$

where the conformal time is defined in terms of the cosmic time as  $d\eta = a^{-1}dt$ . The line element associated to the spatial metric can be given in terms of spherical coordinate,  $\gamma_{ij}dx^i dx^j = dD^2 + D_A^2 d\Omega$ , where  $K$  stands for its constant curvature and the angular diameter distance is defined as  $D_A = K^{-1/2} \sin(K^{1/2}D)$ . For instance, in the  $K \rightarrow 0$  limit,  $\gamma_{ij}$  reduces to the Euclidean one provided  $D_A \rightarrow D$ , describing in this way the flat spatial section of FRW metric. The 0-0 diagonal component of Einstein equation gives the usual Friedmann constraint:

$$H^2 + \frac{K}{a^2} = \frac{\kappa}{3}(\rho_T + \rho_e), \quad (2)$$

where  $\kappa = 8\pi G$ . The balance equations for total matter (including dark matter) and effective dark energy are given by

$$\begin{aligned} \rho'_T &= -3(\rho_T + p_T) + \frac{Q_c}{H}, \\ \rho'_x &= -3(\rho_x + p_x) + \frac{Q_x}{H}. \end{aligned} \quad (3)$$

We can also consider that symbol  $\bar{T} = T - c$  stands for normal matter excluding interacting dark matter, in which case, the balance equations now read

$$\begin{aligned} \rho'_{\bar{T}} &= -3(\rho_{\bar{T}} + p_{\bar{T}}), \\ \rho'_c &= -3(\rho_c + p_c) + \frac{Q_c}{H}, \\ \rho'_x &= -3(\rho_x + p_x) + \frac{Q_x}{H}. \end{aligned} \quad (4)$$

At this point, we define  $\bar{Q}_x = Q_x/H$  and balance equations imply  $\bar{Q}_x = -\bar{Q}_c$ . Since we are interested in solving the system of equations (2)-(4) for determining the dynamic of the universe at background level, we must give some information concerning to the equation of states which obey all kinds of species involved in Friedmann equation. For instance, we assume pressureless dark matter with an equation of state  $w_c = 0$  while effective dark energy has a linear equation of state, thus,  $p_x = w_x \rho_x$  with  $w_x < 0$ .

Let us begin by mentioning the physical guiding principles used for constructing the PPF formalism in a consistent manner [88], [89]. Our point of departure is the well known Einstein equations

$$G^{\mu\nu} = \kappa \sum_I T_I^{\mu\nu} = \kappa(T_{\bar{T}}^{\mu\nu} + T_e^{\mu\nu} + T_c^{\mu\nu}). \quad (5)$$

Here  $I = \{\bar{T}, c, e\}$  and the subscript “ $\bar{T}$ ” stands for the total stress energy tensor excluding dark matter, “ $e$ ” indicates the effective dark energy component, while “ $c$ ” refers to interacting dark matter. Eq. (5) tells us the energy-momentum tensor for dark energy component can

be obtained as the difference between the geometry encoded in the  $G_{\mu\nu}$ -tensor and the energy-momentum tensor of other components (barions, photons, neutrinos, etc.):

$$T_e^{\mu\nu} \equiv \frac{1}{\kappa} G^{\mu\nu} - T_{\bar{T}}^{\mu\nu} - T_c^{\mu\nu}. \quad (6)$$

Taking the covariant derivative at both sides of Eq. (6), using that ordinary matter fulfills  $\nabla_\mu T_{\bar{T}}^{\mu\nu} = 0$  and the Bianchi identities as well, we obtain the following relation between effective dark energy and dark matter

$$\nabla_\mu T_e^{\mu\nu} + \nabla_\mu T_c^{\mu\nu} = \frac{1}{\kappa} \nabla_\mu G^{\mu\nu} - \nabla_\mu T_{\bar{T}}^{\mu\nu} = 0, \quad (7)$$

which is consistent with a phenomenological scenario where the effective dark energy is coupled to dark matter. Consequently, we consider that the covariant form of the energy-momentum transfer can then be written as

$$\nabla_\nu T_I^{\mu\nu} = Q^\nu_I, \quad \sum_{I=e,c} Q^\nu_I = 0, \quad (8)$$

where  $Q^\nu_I$  is a four-vector that takes into account not only the exchange of energy in the dark sector but also the transfer of momentum.

Given the symmetries of FRW metric, the energy-momentum tensor related to any kind of matter only involves the energy density and the pressure

$$T^\mu_\nu = \text{diag}[-\rho, p, p, p]. \quad (9)$$

Our next step is to consider linear perturbations of the FRW background, the Einstein equations, and balance equations as well. To tackle such task, we must follow the standard procedure of splitting the linear perturbations into three different modes: scalar, vector, and tensorial. In doing so, we only pay attention to the scalar mode of the perturbed Einstein equations, expanding the perturbed variables in terms of the eigenfunctions of the Laplace operator [67], [68], [69], thus we call  $Y \equiv Y_k(\mathbf{x}) = e^{i\mathbf{k}\cdot\mathbf{x}}$  to the  $k$ -th eigenfunction (plane-wave) of the Sturm-Liouville problem associated to Laplace operator,  $\nabla^2 Y = -k^2 Y$ . The first and second covariant derivatives of  $Y$  lead to the following two relationships, (i)- $Y_i = -k \nabla_i Y$  and (ii)- $Y_{ij} = \left(\frac{\nabla_i \nabla_j}{k^2} + \frac{\gamma_{ij}}{3}\right) Y$ . In the same manner, the perturbed metric involves four functions called potential  $A$ , shift  $B$ , curvature  $H_L$ , and shear  $H_T$ :

$$\begin{aligned} \delta g_{00} &= -a^2(2AY), \\ \delta g_{0i} &= -a^2 B Y_i, \\ \delta g_{ij} &= a^2(2H_L Y \gamma_{ij} + 2H_T Y_{ij}). \end{aligned} \quad (10)$$

The perturbed energy-momentum tensor is

$$\begin{aligned} \delta T^0_0 &= -\delta\rho, \\ \delta T^0_i &= -(\rho + p)vY^i, \\ \delta T^i_j &= \delta p Y \delta^i_j + p \Pi Y^i_j. \end{aligned} \quad (11)$$

The rhs of Einstein field equations accounts for the total energy-momentum tensor and the same holds for the perturbed Einstein field equations. Because of the additive property of the total energy-momentum tensor, we write the total density perturbation, the total pressure perturbation, or total velocity perturbation in terms of the contribution coming from each species

$$\begin{aligned}\delta\rho &= \sum_i \delta\rho_i, \quad (\rho + p)v = \sum_i (\rho_i + p_i)v_i, \\ \delta p &= \sum_i \delta p_i, \quad p\Pi = \sum_i p_i\Pi_i.\end{aligned}\tag{12}$$

Using (6), (10), and (11), we obtain that the most general form of the Einstein equations is

$$\begin{aligned}H_L + \frac{1}{3}H_T + \frac{B}{k_H} - \frac{H'_T}{k_H^2} &= \\ \frac{\kappa}{2H^2 c_K k_H^2} \left[ \delta\rho + 3(\rho + p) \frac{v - B}{k_H} \right], \\ A + H_L + \frac{H_T}{3} + \frac{B' + 2B}{k_H} \\ - \left[ \frac{H''_T}{k_H^2} + \left( 3 + \frac{H'}{H} \right) \frac{H'_T}{k_H^2} \right] &= - \frac{\kappa}{H^2 k_H^2} p\Pi, \\ A - H'_L - \frac{H'_T}{3} - \frac{K}{(aH)^2} \left( \frac{B}{k_H} - \frac{H'_T}{k_H^2} \right) \\ &= \frac{\kappa}{2H^2} (\rho + p) \frac{v - B}{k_H}, \\ A' + \left( 2 + 2 \frac{H'}{H} - \frac{k_H^2}{3} \right) A - \frac{k_H}{3} (B' + B) \\ - H''_L - \left( 2 + \frac{H'}{H} \right) H'_L &= \frac{\kappa}{2H^2} (\delta p + \frac{1}{3} \delta\rho).\end{aligned}\tag{13}$$

We define  $k_H = (k/aH)$ ,  $c_K = 1 - 3K/k^2$ , and the prime refers to a logarithmic derivative, thus  $' = d/d \ln a$ . The perturbed balance equations for each specie take the form of the continuity and Navier-Stokes equations

$$\begin{aligned}(\rho_i \Delta_i)' + 3(\rho_i \Delta_i + \Delta p_i) - (\rho_i + p_i)(k_H V_i + 3H'_L) \\ &= \frac{\Delta Q_i - \xi Q_i}{H}, \\ \frac{[a^4(\rho_i + p_i)(V_i - B)]'}{a^4 k_H} - \Delta p_i + \frac{2}{3} c_K p_i \Pi_i - (\rho_i + p_i) A \\ &= \frac{a}{k} [Q_i(V - V_T) + f_i].\end{aligned}\tag{14}$$

A general energy-momentum transfer can be split relative to the total four-velocity as

$$Q^\nu_I = Q_I u^\nu + F^\nu_I, \quad Q_I = \bar{Q}_I + \delta Q_I, \tag{15}$$

such that  $u_\nu F^\nu_I = 0$ , where  $Q_I$  is the energy density transfer and  $F^\nu_I$  is the momentum density transfer rate

relative to  $u_\nu$ . Indeed,  $F^\nu_I = a^{-1} \delta^j_i F_I Y^i$  only has spatial component because this momentum transfer potential must be vanish at background level. For scalar perturbations (10), the four vector perturbed velocities are given by

$$\begin{aligned}u_{\mu I} &= a(-1 - AY; (V_I - B)Y_i), \\ u^\mu_I &= a^{-1}(1 - AY; V_I Y^i).\end{aligned}\tag{16}$$

The four vector interaction is then written as

$$Q_{\mu I} = a(-Q_I(1 + YA) - \delta Q_I Y; [F_I + Q_I(V - B)]Y_i), \tag{17}$$

where  $\delta Q_I$  and  $F_I$  stand for the energy transfer perturbation and the intrinsic momentum transfer potential of  $I$ -fluid, which fulfill the standard conservation constraints:

$$\begin{aligned}\sum_I F_I &= 0, \\ \sum_I \delta Q_I Y &= 0.\end{aligned}\tag{18}$$

We highlight that in the interaction term appears index “c” because only dark matter (as an element of the total matter group) interacts with dark energy, the others remain uncoupled. As usual, we choose the comoving gauge  $V_T = B$ , so N-S equation becomes a constraint which determines one of the metric variables in terms of matter variables [88], [89]

$$A = - \frac{\frac{a}{k} [Q_c(V - V_T) + f_c] + \Delta p_T - \frac{2}{3} c_K p_T \Pi_T}{(p_T + p_T)}. \tag{19}$$

We explicitly used  $\sum_k [f_k(x)]' = [\sum_k f_k(x)]'$  with  $k \in \mathbb{N}$  on the last line along with the definition of total momentum:  $(\rho_T + p_T)v_T = \sum_{k \in \mathbb{N}} (\rho_k + p_k)v_k$ .

After having presented all the fundamental equations in the linear perturbation theory, we have to count the number of degree of freedom. The metric perturbation (10) involves four functions ( $A, B, H_L, H_T$ ) while the perturbed matter variables are also four ( $v, \delta\rho, \delta p, \Pi$ ), so we ended with 8-variables. To constraint the aforesaid variables, we have four Einstein equations (13) and two conservation equations (14). In addition, we have two Bianchi identities but also two gauge transformations (one for space coordinate and one for time variable). At the end, we have left two degree of freedom only, which are linked with the pressure fluctuation and anisotropic stress tensor ( $\delta p, \Pi$ ). Therefore some physical assumptions must be done about the latter quantities in order to close the system of equations. In addition, We also must give as an input the covariant form of the interaction.

### III. GAUGE AND ALL THAT

So far, we have worked with the Einstein (13) and balance (14) equations in a general manner without making

any assumption about the metric variables. However, it will be useful within the PPF treatment to employ variables that have clear meaning for gaining some insights about the physics according to gauge selected. Besides, a numerical implementation of the PPF method, as it could be a modification of CAMB code [88], [89], requires to work with a particular gauge.

A gauge transformation establishes a correspondence between the perturbed spacetime and its (background) reference spacetime by means of infinitesimal change of coordinates defined as [67]

$$\begin{aligned}\eta &= \tilde{\eta} + T, \\ x^i &= \tilde{x}^i + LY^i.\end{aligned}\quad (20)$$

The perturbed metric at first order in  $\delta x^\mu = (T, LY^i)$  transforms as

$$g_{\mu\nu}(\eta, x^i) \simeq \tilde{g}_{\mu\nu}(\eta, x^i) + g_{\alpha\nu}\delta x_\mu^\alpha + g_{\alpha\mu}\delta x_\nu^\alpha - g_{\mu\nu,\lambda}\delta x^\lambda$$

which means that the four metric variables are modified as

$$\begin{aligned}A &= \tilde{A} - aH(T' + T), \\ B &= \tilde{B} + aH(L' + k_H T), \\ H_L &= \tilde{H}_L - aH(T + \frac{1}{3}k_H L), \\ H_T &= \tilde{H}_T + aHk_H L.\end{aligned}\quad (21)$$

In addition, the density, pressure, velocity, and anisotropic pressure perturbations under this gauge transformation can be expressed as

$$\begin{aligned}\delta\rho &= \tilde{\delta\rho} - \rho' aHT, \\ \delta p &= \tilde{\delta p} - p' aHT, \\ v &= \tilde{v} + aHL', \\ \Pi &= \tilde{\Pi}.\end{aligned}\quad (22)$$

Once the functions  $T$  and  $L$  are defined without any ambiguity, we can say that the gauge is completely fixed. In order to compare the previous transformation rules with the ones reported by Kodama-Sasaki, we must identify  $T_{\text{Hu}} = T_{\text{KS}}Y$ . For further details about the transformation law of matter variables, the reader can look at Kodama-Sasaki's article, where it is shown that anisotropic stress term is a gauge-invariant quantity [67].

For obtaining a physical interpretation of the PPF method, we must handle with care two different gauges thus we will employ a mix of Newtonian and comoving variables [89]. Let us start by mentioning how the comoving gauge is defined. In the comoving gauge, we identify the shift metric variable with the total velocity  $B = v_T$  while we set the shear function equal to zero ( $H_T = 0$ ). Replacing the latter condition into the transformation for shear variable (21) leads to  $L$  while  $T$  is obtained from the transformation rule for  $B$  using that  $B = v_T$ :

$$T = \frac{(\tilde{v}_T - \tilde{B})}{k}, \quad L = -\frac{\tilde{H}_T}{k}.\quad (23)$$

One of the caveat of working with a mix of gauges is that variable names must be handle with caution. Having mentioned this, it becomes useful to give to the metric variables another labels

$$\begin{aligned}\zeta &\equiv H_L, \quad \xi \equiv A, \quad \rho\Delta \equiv \delta\rho, \\ \Delta p &\equiv \delta p, \quad V \equiv v.\end{aligned}\quad (24)$$

On the other hand, the Newton or conformal gauge is defined by fixing the shear and shift functions equals to zero ( $B = H_T = 0$ ). Inserting the previous conditions into (21) yields

$$T = -\frac{\tilde{B}}{k} + \frac{\tilde{H}'_T}{kk_H}, \quad L = -\frac{\tilde{H}_T}{k}.\quad (25)$$

To avoid embroiling, again, we define new variables  $\Phi \equiv H_L$  and  $\Psi \equiv A$ . It will be useful bear in mind, for later convinience, the explicit link between perturbed metric variables associated to the comoving gauge and those belonging to the Newtonian gauge:

$$\zeta = \Phi - \frac{V_T}{k_H}, \quad \xi = \Psi - \frac{V'_T + V_T}{k_H}.\quad (26)$$

#### IV. PPF METHOD

We have illustrated the covariant treatment of the linear perturbation theory applied to FRW metric, now we are in position to deal with the PPF prescription in the case of the effective dark energy coupled to dark matter. The PPF method relies on two physical assumptions. The curvature perturbations in the comoving gauge remain almost constant on superhorizon scales, pointing out that the derivative of  $\zeta$  deviates from zero because there are corrections coming from the fluctuations of effective dark energy, which appear at second order in the comoving wave number  $k_H$  (cf. [89]).

Using the definitions  $B = V_T$ ,  $H_T = 0$ ,  $\zeta = H_L$ , and  $\xi = A$  in the third Einstein equation (13), we obtain

$$\begin{aligned}\zeta' &= \xi - \frac{K}{(aH)^2} \frac{V_T}{k_H} - \frac{\kappa}{2H^2} [(\rho_e + p_e) \frac{V_e - V_T}{k_H} \\ &\quad + (\rho_T + p_T) \frac{V_T - V_T}{k_H}],\end{aligned}\quad (27)$$

where the last term vanishes because we are working in the comoving gauge with  $B = V_T$ . For the sake of completeness, let us write down the other Einstein equations. The first field equations in the comoving gauge reads

$$\begin{aligned}\zeta + \frac{V_T}{3} &= \frac{\kappa a^2}{2c_K k^2} [\Delta_T \rho_T + \Delta_e \rho_e \\ &\quad + (\rho_e + p_e) \frac{V_e - V_T}{k_H} + (\rho_T + p_T) \frac{V_T - V_T}{k_H}],\end{aligned}\quad (28)$$

whereas the second field equation takes the next form

$$\zeta + \xi + \frac{V_T + 2V'_T}{k_H} = -\frac{\kappa a^2}{k^2} [p_e \Pi_e + p_T \Pi_T]. \quad (29)$$

The fourth Einstein equation reads

$$\begin{aligned} \xi' + (2 + 2\frac{H'}{H} - \frac{k_H^2}{3})\zeta - k_H \frac{V_T + V'_T}{3} - \zeta'' \\ - (2 + \frac{H'}{H})\zeta' = \frac{\kappa a^2}{2(Ha)^2} [\Delta p_T + \Delta p_e + \frac{\Delta \rho_T}{3} + \frac{\Delta \rho_e}{3}]. \end{aligned} \quad (30)$$

Following the seminal article of Hu [89], we propose that the effective dark energy contribution in the large scale limit ( $k_H \rightarrow 0$ ) can be accomodated in terms of a single function called  $f_\zeta(a)$

$$\lim_{k_H \ll 1} \frac{\kappa}{2H^2} (\rho_e + p_e) \frac{V_e - V_T}{k_H} = -\frac{1}{3} c_K f_\zeta(a) k_H V_T, \quad (31)$$

while the derivative of curvature perturbation is slightly modified because the metric variable  $\xi$  has changed (19)

$$\lim_{k_H \ll 1} \zeta' = \xi - \frac{K}{k^2} k_H V_T + \frac{1}{3} c_K f_\zeta k_H V_T, \quad (32)$$

provided the contribution of total matter velocity is of order  $k_H \zeta$  for adiabatic fluctuations. Taking into account the third Einstein equation (27) and the above condition (31), we find behavior of the first derivative of curvature metric variable

$$\begin{aligned} \lim_{k_H \ll 1} \zeta' = -\frac{\frac{a}{k} [Q_c(V - V_T) + f_c] + \Delta p_T - \frac{2}{3} c_K p_T \Pi_T}{(\rho_T + p_T)} \\ - \frac{K}{k^2} k_H V_T + \frac{1}{3} c_K f_\zeta k_H V_T, \end{aligned} \quad (33)$$

where we used the definition of  $\xi$  (19) and  $(Ha)^2 = k^2/k_H^2$  for admending the second term related to  $K$ . We emphasize that the function  $f_\zeta(\ln a)$  is introduced by hand in the PPF method. Using  $V_T = \mathcal{O}(k_H \zeta)$  in Eq. (33), the derivative of  $\zeta$  keeps relatively small provided  $k_H V_T = \mathcal{O}(k_H^2 \zeta)$ .

Our second requisite refers to the behavior of the Newtonian potential variable in the  $k_H \gg 1$  quasistatic limit, thus we demand that the potential must fulfill

$$\lim_{k_H \gg 1} \Phi_- = \frac{\kappa a^2}{2k^2 c_K} \frac{\Delta_T \rho_T + c_K p_T \Pi_T}{1 + f_G(a)}. \quad (34)$$

Here, the function  $f_G$  encodes a modification of Newtonian potential while  $\Phi_- \equiv (\Phi - \Psi)/2$ . In order to conciliate quasistatic limit with large-scale regime we need to incorporate a new function  $\Gamma$  by hand in such way that satisfies a Poisson-like equation in Fourier space

$$\Phi_- + \Gamma = \frac{\kappa a^2}{2c_K k^2} [\Delta_T \rho_T + c_K p_T \Pi_T]. \quad (35)$$

We have to make several steps for obtainig the equation for  $\Phi_-$ . As an example, using the relations defined in

Eqs. (26) we get  $2\Phi_- = (\zeta - \xi) - k_H^{-1} V'_T$ . To link the later expression with the Einstein equations we need to multiply Eq. (28) by a factor two and make its difference with Eq. (29):

$$\begin{aligned} \Phi_- = \frac{\kappa a^2}{2c_K k^2} [\Delta_T \rho_T + \Delta_e \rho_e + 3(\rho_e + p_e) \frac{V_e - V_T}{k_H} \\ + c_K p_e \Pi_e + c_K p_T \Pi_T] \end{aligned} \quad (36)$$

Combining the modified Poisson equation (35) for the Newtonian metric perturbations and (36), we obtain a formal expression for the effective dark energy, which reads

$$\rho_e \Delta_e + 3(\rho_e + p_e) \frac{V_e - V_T}{k_H} + c_K p_e \Pi_e = -\frac{2k^2 c_K}{\kappa a^2} \Gamma. \quad (37)$$

We define the function  $g = \Phi_+/\Phi_- = (\Phi + \Psi)/(\Phi - \Psi)$  to describe deviations from GR, zero deviation means  $g = 0$ , thus, alternative gravity theories can be examined with the help of two metric variables  $\Phi$  and  $\Psi$ . It can be useful to bearing in mind the following expressions (i)-  $\Phi = (g + 1)\Phi_-$  and (ii)-  $\Psi = (g - 1)\Phi_-$  for later convenience. Indeed, using Eqs. (26) we obtain

$$2\Phi_+ = (\xi + \zeta) + \frac{2V_T + V'_T}{k_H}. \quad (38)$$

A more appealing expression for  $\Phi_+$  is found by employing Einstein equation (29):

$$\Phi_+ = -\frac{\kappa a^2}{2k^2} [p_e \Pi_e] - \frac{\kappa a^2}{2k^2} [p_T \Pi_T]. \quad (39)$$

Eq. (39) establishes an explicit constraint between potential perturbations and the anisotropic pressure fluctuation for total matter

$$\Phi_+ = g(a, k) \Phi_- - \frac{\kappa a^2}{2k^2} [p_T \Pi_T], \quad (40)$$

where we have used that Eq. (40) describes the anisotropic pressure fluctuation for dark energy

$$-\frac{\kappa a^2}{2k^2} p_e \Pi_e = g(\ln a, k) \Phi_- . \quad (41)$$

The function  $g = \Phi_+/\Phi_-$  measure the relevance or weakness of the true anisotropic stress (anisotropic pressure fluctuation), and is usually known as the metric ratio parameter.

If one takes  $g = 0$  and  $\Pi_T = 0$ , the source term defined as  $S = \Gamma' + \Gamma$  is simplified in the large-scale limit

$$\begin{aligned} S = \frac{\kappa a^2}{2k^2} \left( \frac{3a}{kc_K} [Q_c(V - V_T) + F_c] + \frac{1}{Hc_K} [\Delta Q_c - \xi Q_c] \right. \\ \left. + V_T k_H [-f_\zeta(\rho_T + p_T) + (\rho_e + p_e)] \right). \end{aligned} \quad (42)$$

A full derivation of this expression can be found in the Appendix A.

Bearing in mind that the  $\Gamma$  function has been introduced for interpolating the large scale regime with the quasistatic phase, then the modified Poisson equation (35) must agree in the small-scale limit with Eq. (34),

$$\lim_{k_H \gg 1} \Gamma = f_G \Phi_- . \quad (43)$$

It is possible to conciliate both limits if the equation of motion for  $\Gamma$  can be written as follows

$$(1 + c_\Gamma^2 k_H^2)[\Gamma' + \Gamma + c_\Gamma^2 k_H^2(\Gamma - f_G \Phi_-)] = S . \quad (44)$$

Here  $c_\Gamma$  corresponds to a new parameter which determines transition scale in terms of the Hubble factor; thus the transition between the large and small scale are obtained by demanding the condition  $c_\Gamma k = \mathcal{H}$ . Note that at  $a \rightarrow 0$ ,  $\Gamma$  vanishes because the source vanishes.

After performing the same kind of lengthy calculations that Hu did in his seminal work [89], the effective dark energy momentum density is obtained

$$\begin{aligned} \kappa a^2 V_e(\rho_e + p_e) = & -2a^2 \mathcal{H} k \frac{g+1}{F(a)} \left( [S_0 - \Gamma - \Gamma'] \right. \\ & \left. + \frac{\kappa a^2}{2k^2} f_\zeta(\rho_T + p_T) V_T k_H \right) + \kappa a^2 V_T(\rho_e + p_e) , \end{aligned} \quad (45)$$

where

$$F(a) = 1 + 3(g+1) \frac{\kappa a^2}{2k^2 c_K} (\rho_T + p_T) . \quad (46)$$

Above, the term  $S_0$  stands for the source expression obtained in the large scale limit ( $k_H \rightarrow 0$ ).

We can use the dark energy Navier-Stokes equation for determining pressure fluctuation  $\Delta p_e$ :

$$\frac{[a^4(\rho_e + p_e)(V_e - V_T)]'}{a^4 k_H} = \Delta p_e - \frac{2}{3} c_K p_e \Pi_e + (\rho_e + p_e) \xi . \quad (47)$$

In this way, it has given all the main ingredients needed for applying the PPF prescription. As it was mentioned before, this method requires as an input the specification by hand of three free functions  $f_\zeta(\ln a)$ ,  $f_G(\ln a)$  and  $g(\ln a, k)$  along with one parameter  $c_\Gamma$ . One should mention that within the PPF framework density perturbation corresponding to dark energy  $\rho_e \Delta_e$  and its perturbed momentum,  $V_e$ , are both derived quantities as it can be seen from Eq. (37) and Eq. (45), respectively. The aforesaid fact could be the key to understand why the method could be useful for curing some existing instabilities in the dark sector; it could keep the growing of effective dark energy perturbation, encoded in the function  $\Gamma$ , considerably small because there is not a master equation for such quantities but mostly we are not forcing a relationship between  $\Delta p_e$  and  $\rho_e \Delta_e$  for closing the system of equations. Of course, in turn, we must specify some functions by hand.

A very useful expression for the source term  $S$  in the synchronous gauge is

$$\begin{aligned} S_{\text{sync}} = & \frac{\kappa a^2}{2k^2} \left( \frac{3a}{kc_K} [Q_c(V - V_T) + F_c]_{\text{sync}} \right. \\ & + \frac{1}{Hc_K} [\Delta Q_c - \xi Q_c]_{\text{sync}} \\ & \left. + k_H(v_T^s + \sigma)[-(\rho_T + p_T)f_\zeta + (\rho_e + p_e)] \right) . \end{aligned} \quad (48)$$

A derivation of Eq. (48) can be found in Appendix B. Such a task requires a long calculation because we must express the source function in the synchronous gauge. We performed a detailed calculation in order to keep the physical aspect as clear as possible, trying to extract some insight from the PPF formalism within the framework of interacting dark sector. The aforesaid steps will be essential for analyzing the perturbation of the models not only within the PPF framework but also in the standard approach (cf. Appendix B).

Having described the main ingredients of the PPF formalism, we must give a “bad” interaction vector, explore the background dynamic and assess the physical consequences coming from the PPF treatment. We start by considering an interaction four-vector  $Q_x^\mu = H\bar{Q}_x u_c^\mu$  with  $Q_x^\mu || u_c^\mu$  as our case I; a similar case was examined in [106]. Here we take  $\bar{Q}_x = -3\xi_c \rho_c$  and identify  $Q_x \equiv aQ_x^0 = H\bar{Q}_x$  as the interaction for the background. Using the energy conservation,  $Q_c^\mu = H\bar{Q}_c u_c^\mu$ , so it can be written covariantly provided the definition of local energy density for dark matter, namely  $T_{\nu c}^\mu u_c^\nu = -\rho_c u_c^\mu$ .

The general form of an interaction vector under linear perturbation is [67]

$$Q_{\mu I} = a(-Q_I(1 + YA) - \delta Q_I Y; [F_I + Q_I(V - B)]Y_i) , \quad (49)$$

where  $\delta Q_I$  and  $F_I$  stand for the perturbed energy transfer and the momentum transfer potential of  $I$ -fluid. As we have already mentioned, these quantities fulfill the standard conservation constraints: (i)-  $\sum_I F_I = 0$  and (ii)-  $\sum_I \delta Q_I Y = 0$ .

The general four-velocity associated to an  $I$ -fluid can be written as

$$u_{\mu I} = a(-1 - AY; (V_I - B)Y_i) , \quad (50)$$

thus, the interaction can be recast as

$$Q_{\mu x} = a\bar{Q}_x H(-1 - AY; (V_c - B)Y_i) . \quad (51)$$

Note that the spatial part of the interaction vector appears  $V_c$  because we have chosen  $Q_x^\mu || u_c^\mu$  from the beginning. Perturbating the  $\bar{Q}_x$  part of (51) at first order yields

$$\begin{aligned} Q_{\mu x} = & aH(\bar{Q}_x + \delta\bar{Q}_x)(-1 - AY; (V_c - B)Y_i) \\ \equiv & aH(-(1 + AY)\bar{Q}_x - \delta\bar{Q}_x; \bar{Q}_x(V_c - B)Y_i) . \end{aligned} \quad (52)$$



Comparing with the general case (49), we obtain  $\delta Q_x = \delta Q_x Y$  which does not give any new information because  $Y$  is a re-scale function which appears here because of Kodama-Sasaki convention [67], however, its spatial part leads to  $F_x = Q_x(V_c - V) = -F_c$  with  $\delta Q_x = H\delta\bar{Q}_x = -\delta Q_c$ . We assume that  $\xi_c H$  could be related with interaction rates that vary only with time; so a characteristic scale could be given by  $\tau_c^{-1} = \xi_c H$  in the decay of dark matter into dark energy. We also neglect space-like variation  $\delta H$ . If  $V_c = V$  then  $F_x = 0$ .

We consider  $Q_x^\mu = H\bar{Q}_x u_x^\mu$  so  $Q_x^\mu || u_x^\mu$  with  $Q_x \equiv aQ_x^0 = -3H\xi_c\rho_c$  as our case II. Following the same steps, we write the interaction vector

$$\begin{aligned} Q_{\mu x} &= a(-(1 + AY)Q_x - \delta Q_x; Q_x(V_x - B)Y_i) \\ &\equiv a(-Q_x(1 + YA) - \delta Q_x Y; [F_x + Q_x(V - B)]Y_i). \end{aligned} \quad (53)$$

The only change is introduced by the momentum transfer potential; thus, comparing the spatial components in (53), we find  $F_x = Q_x(V_x - V) = -F_c$ . The previous case was not analyzed in [106].

As a closing remark, the background equations for the interacting dark sector are obtained by solving their balance equations or employing another method developed in [87]:

$$\begin{aligned} \rho_x &= \rho_{x0}a^{-3(1+w_x)} + \frac{\xi_c}{w_c - w_x - \xi_c}\rho_{c0}a^{-3(1+w_c-\xi_c)} \\ \rho_c &= \rho_{c0}a^{-3(1+w_c-\xi_c)}. \end{aligned} \quad (54)$$

For  $w_c = 0$  and  $w_x = -1$ , in the limit of vanishing coupling, we recover the vanilla model. This means that our model is not able to mitigate the coincidence problem provided the inverse of ratio  $\rho_c/\rho_x$  leads to

$$\frac{r_0}{r} = a^{-3(\xi_c+w_x-w_c)} + \frac{\xi_c}{-w_x-\xi_c}, \quad (55)$$

where  $r_0$  refers to its value today. For  $\xi_c > w_x$ , (55) reaches a positive constant value in the small scale factor limit while for large scale factor the ratio  $\rho_c/\rho_x$  asymptotically vanishes, which is an obstacle for avoiding the coincidence problem and we will not address such issue here. Our goal is to examine the aforesaid background within the interacting PPF formalism taking into account different choice in the momentum transfer potential. More specifically, we would like to understand the physical signature in choosing different momentum transfer potentials and its impact on parameter estimation of the coupling strength or  $\tau_c$  parameter. Regarding the background dynamic, energy densities (54) are good enough to reproduce standard sequences of eras for the universe: radiation-barions-dark matter-dark energy.

In summary, an exchange of energy proportional to dark matter leads to unstable perturbations within the standard perturbation theory [78], however, an appealing method for avoiding this well known large scale instability at early time seems to be PPF formalism [106]. Our next step is to confront the previous theoretical model with observational data.

## V. OBSERVATIONAL CONSTRAINTS

### A. Data and Methodology

We perform a statistical estimation of the cosmic parameters by using the Markov Chain Monte-Carlo method with help of public code CosmoMC [73]. In doing so, we modify the PPF patch developed in [91] by including an interaction between dark matter and effective dark energy within the PPF formalism [106].

Before going any further with the statistical analysis, let us summarize the sort of data used for the parameter estimation. We will consider the data coming from type Ia supernovae, cosmic microwave background anisotropies, barionic acoustic oscillation along with redshift space distortion. Regarding the standard candles, we will take into account the ‘‘JLA compilation’’ composed of 740 supernovae because it is the largest data set available which contains samples from low redshift  $z = 0.02$  to large one, near  $z \simeq 1$ , spanning an excellent cosmic window for examining the evolution of the universe. Such data were obtained from the joint analysis of SDSS II and SNLS [31], improving the analysis by means of a recalibration of light curve fitter SALT2 and in turn reducing possible systematic errors.

Temperature anisotropies in the cosmic microwave background provide an important probe for testing any cosmological model. We include the multipole measurements obtained by WMAP9 team [1] along with the recent data released by Planck satellite [2], [3], [4] which extends the previous one by incorporating low multipoles measurements. Indeed, WMAP9 project involved the measurements of Atacama Cosmology Telescope (ACT) in the range of multipoles  $\ell \in [500, 10000]$  along with the South Pole Telescope (SPT) observations which reported data over the range  $\ell \in [600, 3000]$ . Planck survey performed measurements over a complementary zone,  $\ell \in [2, 2500]$ ; being the main source of error at  $\ell < 1500$  the cosmic variance. Planck power spectra are separated in three different zones. The temperature fluctuations at low multipoles,  $\ell \in [2, 49]$ , corresponds to the  $C_l^{TT}$  mode and is analyzed under the Commander Bayesian approach; the temperature fluctuations and polarisation analysis are performed for  $\ell \in [2, 32]$  in the low-like scheme including  $C_l^{TE}$ ,  $C_l^{EE}$ , and  $C_l^{BB}$  components. From 50 to 2500 multipoles, the CMB power spectrum involves CAMspec method, which examines the  $C_l^{TT}$  mode also [3]. Interestingly enough, Planck data alone give considerably tighter bounds over the cosmological parameters than those from the WMAP9 data [3] or a combination of SPT and ACT observations with WMAP9 data.

An imprint of primordial barionic acoustic oscillation (BAO) can be detected in several galaxy surveys by taking into account the acoustic peak scale related with the two-point correlation function of galaxies or its related

$z$	$f\sigma_8(z)$	Survey	Reference
0.067	$0.42 \pm 0.06$	6dFGRS (2012)	[8]
0.17	$0.51 \pm 0.06$	2dFGRS (2004)	[5]
0.22	$0.42 \pm 0.07$	WiggleZ (2011)	[12]
0.25	$0.39 \pm 0.05$	SDSS LRG (2011)	[15]
0.37	$0.43 \pm 0.04$	SDSS LRG (2011)	[15]
0.41	$0.45 \pm 0.04$	WiggleZ (2011)	[12]
0.57	$0.43 \pm 0.03$	BOSS CMASS (2012)	[6]
0.60	$0.43 \pm 0.04$	WiggleZ (2011)	[12]
0.78	$0.38 \pm 0.04$	WiggleZ (2011)	[12]
0.80	$0.47 \pm 0.08$	VIPERS (2013)	[13]

TABLE I: Compilation of  $f\sigma_8(z)$  data points obtained from several galaxy surveys using RSD method. Some of data points were considered in [15], [16]. The value of  $f\sigma_8(z)$  at  $z = 0.8$  was reported by the VIPERS survey [13].

partner, the matter power spectrum. Indeed, this scale can be used as a cosmic ruler by measuring the distance to objects at a given redshift in terms of the comoving sound horizon at recombination, therefore, the reported value of the distance ratio  $d_z = r_s(z_d)/D_V(z)$  with its error at different redshifts turned to be considered as another useful constraint. For instance, the 6dFGS mission informed the value of  $d_z(0.106)$  [9], SDSS-DR7 measured  $d_z(0.35)$  [10], SDSS-DR9 exploration led to  $d_z(0.57)$  [11], and diverse measurements from the WiggleZ dark energy survey reported  $d_z(0.44)$ ,  $d_z(0.60)$ , and  $d_z(0.73)$ , respectively [12]. In this same context, it has been designed a complementary tool for testing dark energy based on the redshift space distortions (RSD) technique [14], [15]. The measurements of the quantity  $f(z)\sigma_8(z)$  at different redshifts unifies the cosmic growth rate  $f$  and the matter power spectrum  $\sigma_8$  normalized with the comoving scale  $8h^{-1}$  Mpc, in a single quantity which includes the latest results of galaxy surveys such as 6dFGS, BOSS, LRG, WiggleZ, and VIPERS [see Table (I)]. The  $f(z)\sigma_8(z)$  test has been used for constraining holographic dark energy model and DGP cosmology [17]. In particular, these observational data were combined with the Planck data for obtaining stringent bounds on the growth index for the concordance model or a deviation from GR theory [18], likewise helped to improve the constraints on warm dark matter equation of state [19] or interacting dark fluid with constant adiabatic speed sound [20]. Besides, a comparative analysis was carried out for the vanilla model with different parametrization of the growth index including an overall likelihood analysis with SNeIa+BAO+CMB+Growth data a few years ago [21] (see also [22] for related issues). For all these reasons, we think it will be useful to take into account these data in our forthcoming analysis. In contrast with previous work [106], our data sets contain the largest JLA compilation of supernovae and the latest measurements of the quantity  $f(z)\sigma_8(z)$ , while the other probes corresponding to CMB power spectrum with WMAP9-Planck data and BAO distance measurements are similar. Most importantly, we set  $c_T$  as a free parameter, within the

Data	Magnitude
CMB	WMAP9+Planck: $C^{TT}, C^{TE}, C^{EE}, C^{BB}$
SNeIa	JLA: $\mu(z)$
BAO	DR9-DR7-6dFGS: $d_z = r_s(z_d)/D_V(z)$
HST	Hubble: $H_0$
RSD	Growth data: $f(z)\sigma_8(z)$

TABLE II: List of data sets used in the likelihood analysis with MCMC method.

PPF formalism, to be constrained under the combined likelihood analysis and to test its impact or maybe its correlation with other physical parameters as could be the interaction coupling.

Our methodology is to employ a modified version of CosmoMC package [73] for implementing a Markov chain Monte-Carlo analysis of the parameter space, in the PPF formalism with an exchange of energy-momentum between dark matter and dark energy, using CMB data from WMAP9 [1] plus Planck [3], JLA compilation of SNe Ia [31], distance measurements for BAO [9], [10], [11], [12], and redshift space distortions through the quantity  $f(z)\sigma_8(z)$  [18], [19] (see Table (II)). We explore a parameter space given by

$$\mathcal{P} = \{\Omega_b h^2, \Omega_c h^2, 100\theta_{MC}, n_s, \ln(10^{10} A_s), \tau, w_x, \xi_c, c_T\}, \quad (56)$$

where  $\Omega_b h^2$  refers to the fraction of baryon in units of  $h$ ,  $\Omega_c h^2$  is the amount of cold dark matter also in units of  $h$ ,  $\theta$  is an approximation to  $r_s/D_A$ ,  $n_s$  is scalar spectral index,  $\ln(10^{10} A_s)$  accounts for amplitude of scalar spectrum,  $\tau$  stands for the reionization optical depth,  $w_x$  refers to dark energy equation of state,  $\xi_c$  indicates the coupling strength, and  $c_T$  is PPF parameter related with a transition scale. We took as prior for the previous parameters the following intervals:  $\Omega_b h^2 \in [0.005, 0.1]$ ,  $\Omega_c h^2 \in [0.001, 0.99]$ ,  $100\theta_{MC} \in [0.5, 10.0]$ ,  $n_s \in [0.5, 1.5]$ ,  $\ln(10^{10} A_s) \in [2.4, 4]$ ,  $\tau \in [0.01, 0.8]$ ,  $w_x \in [-1.5, 0]$ ,  $\xi_c \in [-1, 0]$ , and  $c_T \in [0, 1]$ . Notice that the fraction of dark energy ( $\Omega_x$ ), the amount of dark matter,  $\Omega_m$ , and the age of the universe are all derived parameters.

We adopt the  $\chi^2$  distribution for constraining the parameters, which can be written in terms of the likelihood function as  $-2 \ln \mathcal{L}$ . For the JLA compilation of SNe Ia, the probability distribution is written as

$$\chi^2_{\text{SNe}} = [\mathbf{m}^{\text{obs}} - \mathbf{m}^{\text{th}}]^T \mathbf{C}_{\text{SNe}}^{-1} [\mathbf{m}^{\text{obs}} - \mathbf{m}^{\text{th}}]. \quad (57)$$

Here  $\mathbf{C}$  corresponds to a large covariance matrix given in [31]. The distance modulus is  $\mathbf{m}^{\text{th}} = 5 \log_{10}[d_L(z)/10 \text{ pc}]$ ,  $d_L$  being the distance by luminosity. These photometric events of supernovae take into account two main effects, the time stretching of light curves encoded in the parameter  $\mathcal{X}$  and the supernovae color at the maximum brightness dubbed  $\mathcal{C}$ :

$$\mathbf{m}^{\text{th}} = \mathbf{m}^* - \mathbf{M} + \alpha \mathcal{X} - \beta \mathcal{C}, \quad (58)$$

where  $m^*$  stands for the peak-light measured in the rest-frame B-band for each event while  $\alpha$ ,  $\beta$ , and  $M$  are taken as nuisance parameters, respectively.

For BAO distance measurement (standard ruler), we have that the distribution can be constructed as

$$\chi^2_{\text{BAO}} = [y^{\text{obs}} - y^{\text{th}}]^T C_{\text{BAO}}^{-1} [y^{\text{obs}} - y^{\text{th}}], \quad (59)$$

where  $y^{\text{obs}}$  is the data vector,  $y^{\text{th}}$  contains the theoretical formulae, and  $C_{\text{BAO}}^{-1}$  stands for the inverse covariance matrix for the data vector [3]. Specifically speaking, the components of data vector are given by  $D_V(0.106) = (457 \pm 27)\text{Mpc}$ ,  $r_s/D_V(0.20) = 0.1905 \pm 0.0061$ ,  $r_s/D_V(0.35) = 0.1097 \pm 0.0036$ ,  $A(0.44) = 0.474 \pm 0.034$ ,  $A(0.60) = 0.442 \pm 0.020$ ,  $A(0.73) = 0.424 \pm 0.021$ ,  $D_V(0.35)/r_s = 8.88 \pm 0.17$ , and  $D_V(0.57)/r_s = 13.67 \pm 0.22$ ;  $D_V$  is the effective volume distance while  $A$  is the acoustic parameter; the definition of the aforesaid functions can be found in [3].

The growth data involve the linear perturbation growth factor  $\delta_m$  in terms of the function  $f = d\ln \delta_m / d\ln a$  along with the rms density contrast within an  $8\text{Mpc h}^{-1}$  volume related with the matter power spectrum (see [107]). Using the redshift space distortion, the quantity  $f(z)\sigma_8(z)$  can be measured [18] and therefore can be used as a stringent statistical estimator:

$$\chi^2_{\text{RSD}} = \sum_i \frac{[f\sigma_8^{\text{th}}(z_i) - f\sigma_8^{\text{obs}}(z_i)]^2}{\sigma_i^2}. \quad (60)$$

The inclusion of RSD measurement through growth data implies to add a new module to *CosmoMc* package. Besides, the different contributions to the likelihood function due to the CMB data [3], mentioned at the beginning of this section, are included in the next estimator

$$\chi^2_{\text{CMB}} = \sum_{(\ell, \ell')} [C_{\ell}^{\text{data}} - C_{\ell}^{\text{th}}] M_{\ell\ell'}^{-1} [C_{\ell'}^{\text{data}} - C_{\ell'}^{\text{th}}], \quad (61)$$

where  $\ell_{\min} \leq \ell, \ell' \leq \ell_{\max}$  and  $M_{\ell\ell'}$  stands for the covariance matrix [3]. We consider a Gaussian prior for the current Hubble constant given by [108]. At this point, we will consider all data sets as independent ones so the total distribution is given by

$$\chi^2_{\text{total}} = \chi^2_{\text{SNe}} + \chi^2_{\text{BAO}} + \chi^2_{\text{RSD}} + \chi^2_{\text{CMB}} + \chi^2_{\text{HST}}. \quad (62)$$

We apply the Gelman-Rubin criteria,  $\mathcal{R} - 1 < 0.01$ , for evaluating the reliability of Monte Carlo process in order to assure that the mean estimator in each chain is small compared to the standard deviation for the eight ran chains, implying the accuracy on the confidence intervals [73]. The whole process was performed in the Computing Cluster for Cosmos (CCC).

In the next Subsection, we will compare the outcome of statistical process for vanishing transfer momentum and non-vanishing transfer momentum as well, taking into account the specific four vector interaction presented in Sect. IV.

Parameters	Mean with errors	Best fit
$\Omega_b h^2$	$0.02253178^{+0.00033787}_{-0.00034093}$	0.02255553
$\Omega_c h^2$	$0.12047535^{+0.00222956}_{-0.00221724}$	0.11916320
$100\theta_{MC}$	$1.04136416^{+0.00057296}_{-0.00057710}$	1.04114800
$\tau$	$0.07983820^{+0.01148588}_{-0.01290776}$	0.07798691
$w_x$	$-1.22272129^{+0.07501853}_{-0.07467723}$	-1.16388500
$\xi_c$	$0.00140088^{+0.00079890}_{-0.00080122}$	0.00092117
$c_\Gamma$	---	---
$\ln(10^{10} A_s)$	$3.05966284^{+0.02220724}_{-0.02262323}$	3.05628700
$n_s$	$0.96337319^{+0.00586441}_{-0.00592465}$	0.96472830
$H_0$	$72.56925013^{+1.31515397}_{-1.31569714}$	71.95068000
$\Omega_\Lambda$	$0.72695703^{+0.01069503}_{-0.01068753}$	0.72500170
$\Omega_m$	$0.27304297^{+0.01068753}_{-0.01069485}$	0.27499830
Age/Gyr	$13.78446815^{+0.05272355}_{-0.05300623}$	13.76048000

TABLE III: Constraints on the cosmological parameters using the joint statistic of JLA+Planck+WP+RSD+BAO+HST data in the zero momentum transfer potential case.

## B. Results

Let us start by comparing our results with the ones reported by Y.H. Li *et al.* [106] when the momentum transfer potential vanishes (see Fig. (1)). It is important to remark that our observational constraint can be considered as a complementary analysis provided we have included largest compilation of supernovae events (JLA sample), taken into account the observation of WiggleZ dark energy survey for BAO measurements along with the RSD measurements, improving in this way the quality of the cosmic constraint. Table (III) tells us the interaction coupling is  $\xi_c = 0.00140^{+0.00079}_{-0.00080}$  at  $1\sigma$  level, which shows a relative difference around 0.022% with the estimation found in [106]. Regarding the dark energy equation of state, we have found a lower value for its magnitude, corresponding to a relative difference not bigger than 0.004% in relation to the value mentioned in [106], indeed, a similar kind of effect is propagated to other parameters such the amount of dark energy and dark matter. In addition, we would like to emphasize that the MCMC statistical analysis favors a dark energy equation of state in the phantom zone ( $w_x < -1$ ), implying the amount of dark energy will continue to growing for large scale factor while the dark matter fraction will fade away together with the other components [see Eq. (54)].

One of the main issue of the PPF formalism is how to determine the transition-scale parameter  $c_\Gamma$ . Then, we consider it as a free model parameter, and it turned out to be that its posterior probability distribution (see Fig. (1)) does not exhibit any well defined peak, only a flat shape, showing that any value between zero and the unity are physically admissible. For the latter reason, we will fix at  $c_\Gamma \simeq 0.49$  for the non-zero transfer of momentum case (see Appendix B for further detail). The combined

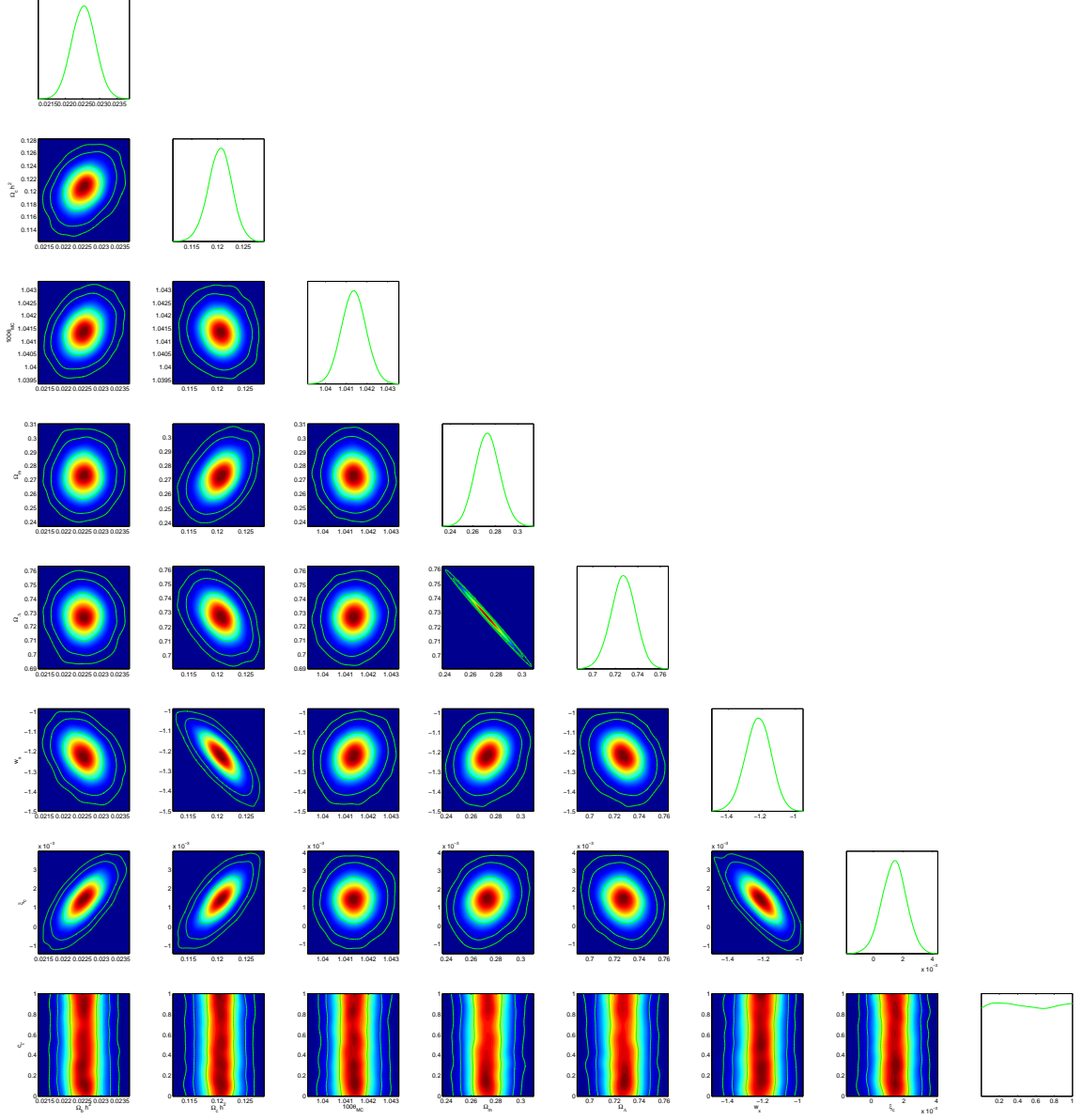


FIG. 1: Joint two-dimensional marginalized constraints on parameter space along with 1D marginalized distribution on each parameter (posterior distribution). These contours combine JLA+Planck+WP+RSD+BAO+HST data. Green lines denote  $1\sigma$ ,  $3\sigma$ , and  $3\sigma$  regions. In this case, the momentum transfer potential vanishes.

analysis of Planck + WP + JLA + BAO + HST + RSD data leads to  $\xi_c = 0.00136^{+0.00080}_{-0.00073}$  at  $1\sigma$  level [see Table (IV) and Fig. (2)], showing a good agreement with previous estimation [106]. As we expected in both cases, the interaction coupling is considerably small because

the concordance model is recovered within our framework by taking  $w_x = -1$ ,  $w_c = 0$ , and  $\xi_c = 0$ , so we do not departure much from it, thus, the joint analysis of Planck + WP + JLA + BAO + HST + RSD data ruled out large interaction coupling,  $\xi_c$ . The main impact of

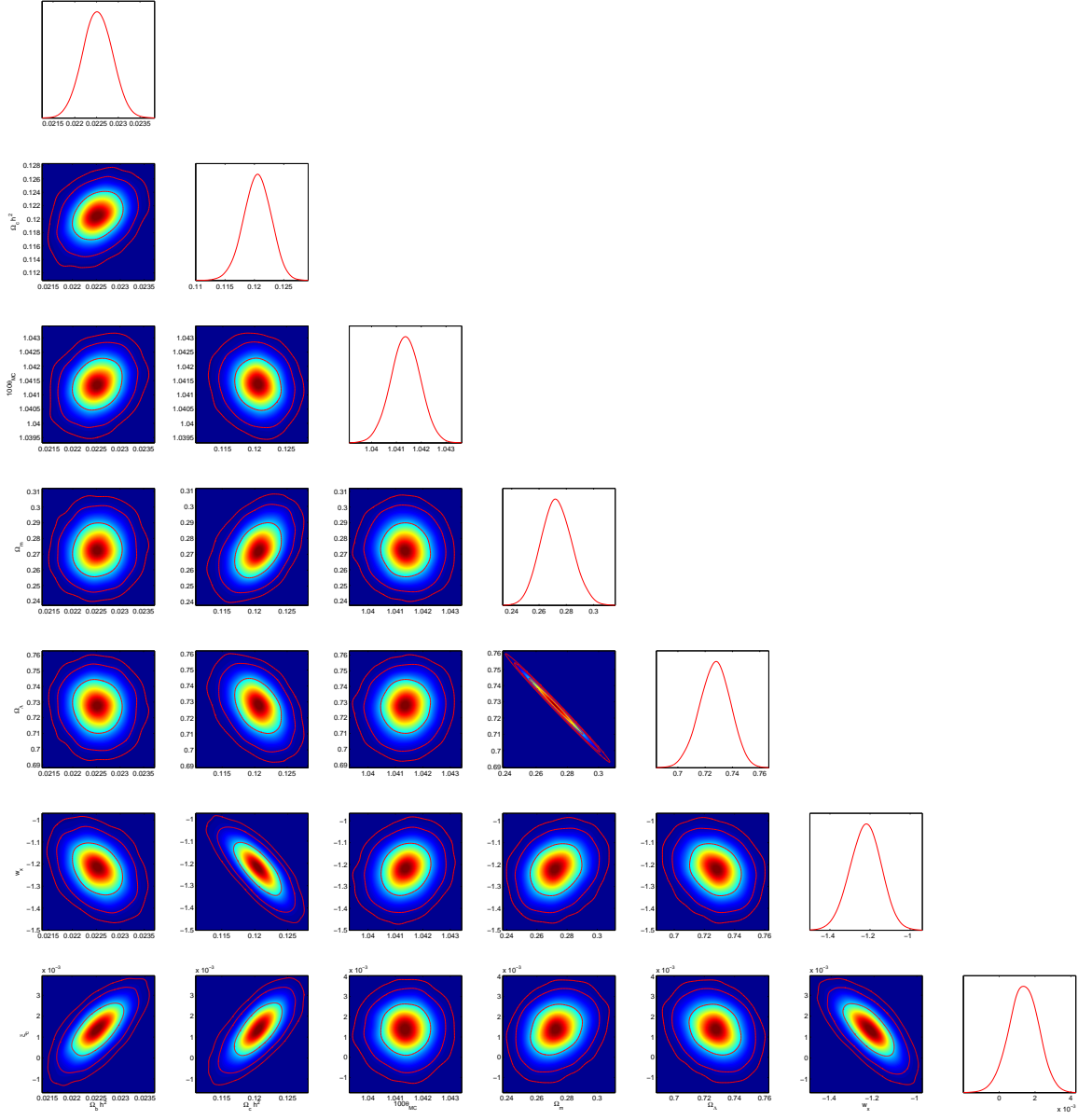


FIG. 2: Joint two-dimensional marginalized constraints on parameter space along with 1D marginalized distribution on each parameter. These contours combine JLA+Planck+WP+RSD+BAO+HST data. Red lines denote  $1\sigma$ ,  $3\sigma$ , and  $3\sigma$  regions. The momentum transfer potential is non-zero.

transfer of momentum is to reduce the interaction coupling in the dark sector, giving arise a relative difference around 0.025%. Further, similar effects can be observed in the fraction of dark matter and dark energy also (see Fig. (2)). Having said this, we must compare our esti-

mation with previous results in literature by taking into account the effect introduced by PPF formalism and the observational data as well. Fig. (3) shows the contrast between our estimation of dark energy amount at present and other results, including Planck alone, JLA sample

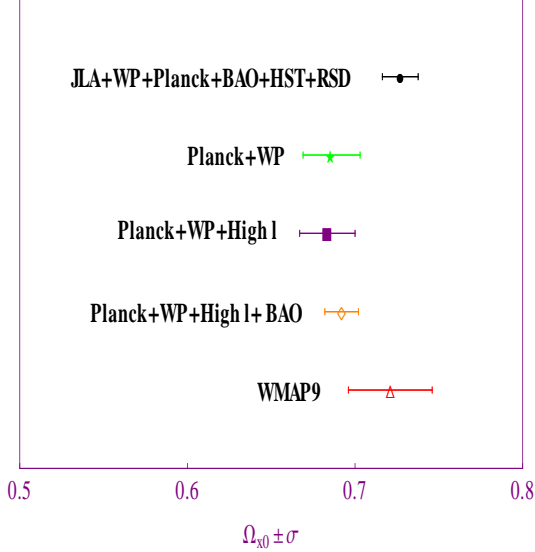


FIG. 3: The estimation of dark energy fraction taking into different observational data sets including our result (black line).

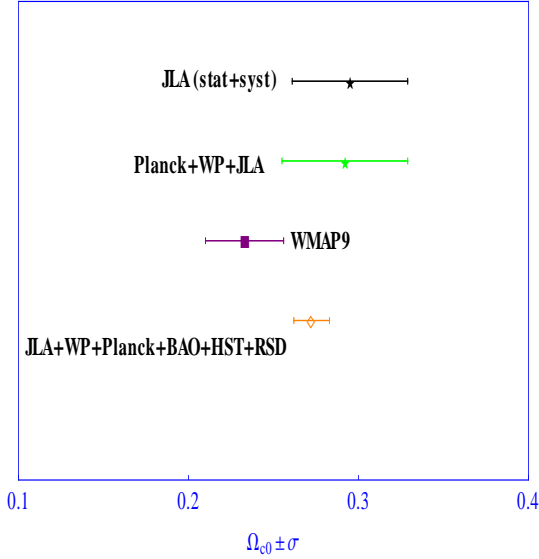


FIG. 4: The estimation of dark matter amount from different observational data sets including our result (orange line).

and WMAP9 observation. For instance, the relative difference for dark energy fraction between our first case and the WMAP9 result alone [1],  $\Omega_{\Lambda} = 0.721 \pm 0.025$ , is very small, 0.008% only. Comparing with the combined analysis of Planck + WP, we obtain a bigger relative difference, 0.061%. Concerning dark matter amount, the most significant difference is obtained with WMAP9 data alone [1], almost 0.17%. Meanwhile, the relative difference with the JLA data alone is not bigger than

Parameters	Mean with errors	Best fit
$\Omega_b h^2$	$0.02252361^{+0.00033315}_{-0.00032982}$	0.02249296
$\Omega_c h^2$	$0.12046346^{+0.00230013}_{-0.00227203}$	0.12020980
$100\theta_{MC}$	$1.04136777^{+0.00057473}_{-0.00057473}$	1.04126800
$\tau$	$0.07930583^{+0.01174373}_{-0.01177567}$	0.07526672
$w_x$	$-1.22222557^{+0.07490911}_{-0.07549658}$	-1.23337100
$\xi_c$	$0.00136585^{+0.00080604}_{-0.00079529}$	0.00152430
$\ln(10^{10} A_s)$	$3.05895257^{+0.02221646}_{-0.02227143}$	3.04931400
$n_s$	$0.96324014^{+0.00579488}_{-0.00581391}$	0.96646290
$H_0$	$72.59170280^{+1.34184153}_{-1.34867459}$	72.87842000
$\Omega_{\Lambda}$	$0.72715554^{+0.01098111}_{-0.01102359}$	0.73010580
$\Omega_m$	$0.27284446^{+0.01097975}_{-0.01097975}$	0.26989420
Age/Gyr	$13.78213201^{+0.05338059}_{-0.05303086}$	13.79356000

TABLE IV: Constraints on the cosmological parameters using the joint statistic of JLA+Planck+WP+RSD+BAO+HST data for the non-vanishing momentum transfer potential case.

0.055% as can be seen from Fig. (4).

After having examined the statistical outcome given by the MCMC method, we are in position to explore the impact of the interaction coupling in the power spectrum. From Fig. (5), we observe that our best fit cosmology does not deviate considerably from the vanilla model. However, increasing the interaction strength leads to an increment in the first peak's height. A useful quantity to characterize the position of the CMB power spectrum first peak is the shift parameter  $R = \sqrt{\Omega_m} \int_0^{z_{rec}} H^{-1}(z) dz$ . Then, reducing the coupling parameter  $\xi_c$  leads to an augment of dark matter fraction at early time (see Fig. (6)) so there must be a shift in the first peak provided  $R \propto \sqrt{\Omega_m}$ . In another way, Fig. (5) tells us that the position of the first peak corresponds to  $\ell_{1peak} \simeq 221$  which is consistent with WMAP9 result,  $\ell_{1peak} = 220.1 \pm 0.8$  [1]. At the low-multipoles ( $\ell < 10$ ) the power spectrum is also affected by the strength of coupling because its amplitude decreases in relation with the concordance model. At large-multipoles ( $\ell > 10^3$ ) our model can be discriminated from it because the power spectrum amplitude increases as can be noticed in the second peak's height. We assess the relative difference between our models for different values of  $\xi_c$  and the vanilla one by taking into account  $\Delta C_l / C_l^{TT}$ . This quantity measures a small deviation which is not bigger than 0.2% [see Fig. (7)]. Our best-fit cosmology with  $\xi_c = 0.0014$  deviates in a 0.05% from the standard model within the range  $\ell \leq 600$ , such difference reaches a 0.1% at  $\ell \simeq 1200$  but it does not become bigger than 0.2% (in module) at large multipoles.

## VI. SUMMARY

We have re-examined the PPF formalism within the interacting dark sector framework by taking into account an interaction proportional to dark matter density. As it was shown in [106], this model can avoid large-scale instability at early time when the treatment of dark energy perturbation is altered provided the relationship between the pressure and density fluctuation for dark energy is

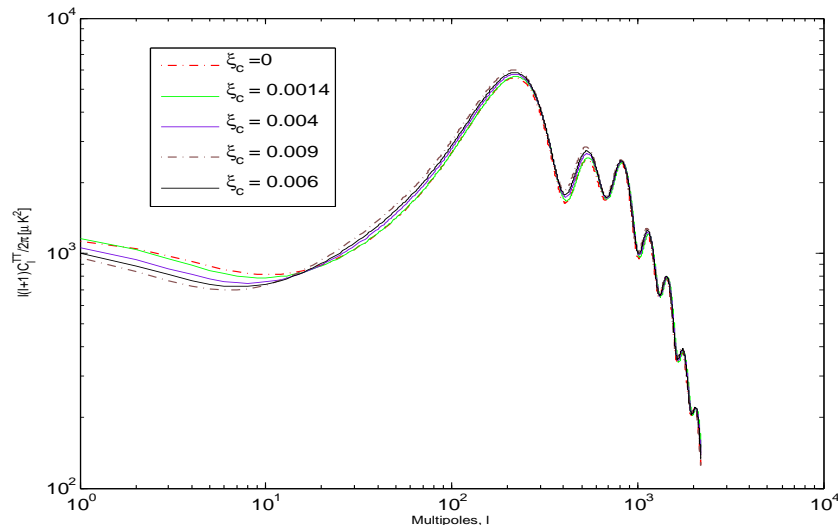


FIG. 5: Power spectrum  $C_l^{TT}$  versus multipoles for different values of interaction coupling,  $\xi_c$ . The vanilla model corresponds to red dash-dot line while our best-fit cosmology is marked with a green solid line. We use in both axes logarithmic scale.

not forced by hand. Another interesting point regarding the PPF approach is that dark energy density and velocity perturbations become both derived concepts [88], [89] in the sense that all physical information about effective dark energy is encoded in a new function called  $\Gamma$  along with its master equation (see Appendices A and B); giving arise a smooth interpolation between the large scale and small scale limits. We have extended previous results by considering non-vanishing momentum transfer potential and recovered similar results for the zero momentum transfer potential case.

We have implemented a MCMC method using a modified version of CosmoMC package [72], [73] including the PPF patch [91] for determining observational bounds on the cosmic parameters [see Figs. (1)-(2)]. In doing so, we have improved the quality of cosmological constraint by employing largest compilation of supernovae events (JLA sample) and adding the observation of WiggleZ dark energy survey for BAO measurements along with the RSD measurements [see Table (III)-(IV)]. When the momentum transfer potential vanishes, the coupling parameter is  $\xi_c = 0.00140^{+0.00079}_{-0.00080}$  at  $1\sigma$  level, showing a difference no bigger than 0.022% with the estimation

reported by other authors [106]. In the non-vanishing momentum transfer potential case, the joint statistic of Planck + WP + JLA + BAO + HST + RSD data gives  $\xi_c = 0.00136^{+0.00080}_{-0.00073}$  at  $1\sigma$  level [see Table (IV) and Fig. (2)], and therefore the transfer of momentum helped to reduce the coupling parameter. In both cases, the combined Planck + WP + JLA + BAO + HST + RSD data ruled out large coupling parameter. Besides, we found that the posterior probability distribution for the transition-scale parameter is mostly flat (see Fig. (1)).

We have compared our statistical analysis with the outcome of different data sets. For instance, the joint analysis of Planck + WP + JLA + BAO + HST + RSD data leads to a dark energy amount which differs in 0.008% with respect to the result reported by WMAP9 alone [1] [cf. Fig. (3)]. In the case of dark matter fraction, the most significant difference concerns to the WMAP9 data alone [1], about 0.17% [cf. Fig. (4)]. It is important to emphasize that aforesaid disagreement are relieved once WMAP9 data are combined with BAO measurements and other probes.

A useful manner to explore the impact of PPF formalism is looking at shape and position of peaks in the CMB

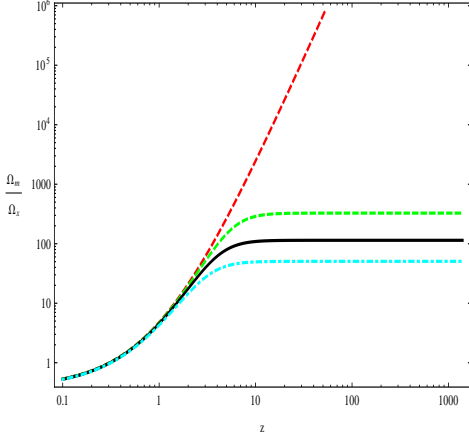


FIG. 6: Ratio  $\Omega_m/\Omega_x$  in terms of redshift with logarithmic scale in both axes. Red lines corresponds to vanilla model, green line is our best cosmology with  $\xi_c = 0.0014$ , black line represents  $\xi_c = 0.004$  case while cyan line is for  $\xi_c = 0.009$ . The amount of dark matter in relation to dark energy fraction is increased by augmenting  $\xi_c$ .

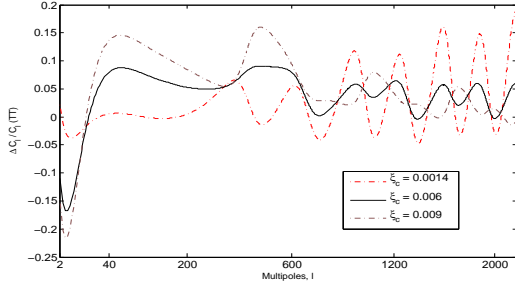


FIG. 7: Relative difference  $\Delta C_l/C_l^{TT}$  versus multipoles for different values of interaction coupling,  $\xi_c$ .

power spectrum. In doing so, we found there is a correlation between the the first peak's height and the value taken by coupling parameter  $\xi_c$ . The amplitude of this peak is slightly amplified when  $\xi_c$  reaches higher values within the range  $[0, 0.009]$  [see Fig. (5)]. The position of this peak is also altered because it depends on the amount of dark matter, which aguments at early times. As can be noticed from Fig. (5), the amplitude of all peaks is altered in relation with the vanilla model. In

fact, we use  $\Delta C_l/C_l^{TT}$  as an estimator for evaluating the contrast between the vanilla model and our best-fit cosmology [see Fig. (7)], roughly speaking, such deviations are kept below 0.2% in the full range of multipoles.

## Acknowledgments

L.X is supported in part by NSFC under the Grants No. 11275035 and “the Fundamental Research Funds for the Central Universities” under the Grants No. DUT13LK01. M.G.R is partially supported by CON-ICET. We acknowledge the use of the CAMB and CosmoMC packages [72], [73]. We acknowledge the use of CCC for performing the statistical analysis.

## Appendix A: Deriving the source equation

In this section, we will outline the main steps to derive the general source term in the case of interacting dark energy models. In order to make the treament self-consistent, we must determine a master equation for  $\Gamma$  which takes into account the two prerequisites (33) and (34). In doing so, we must fill some gaps in the original derivation. We start by taking derivative of Eq.(26) and using  $\Phi = (g+1)\Phi_-$  in (26)

$$\zeta' = \Phi' - \left(\frac{V_T}{k_H}\right)' = g'\Phi_- + (g+1)\Phi'_- - \left[\frac{V_T'}{k_H} - \frac{V_T}{k_H} \left(\frac{k_H'}{k_H}\right)\right]. \quad (A1)$$

From its own definition, we can show the next relation:

$$\frac{k_H'}{k_H} = -\left(1 + \frac{H'}{H}\right). \quad (A2)$$

In fact, inserting (A2) into (A1) helps us to cast (A1) in a simpler form

$$\zeta' = g'\Phi_- + (g+1)\Phi'_- - \frac{V_T'}{k_H} + \frac{V_T}{k_H} \left(1 + \frac{H'}{H}\right). \quad (A3)$$

With the help of Eq.(26), we obtain  $V_T'/k_H = -[\xi - (g-1)\Phi_- + V_T/k_H]$  which later is replaced in Eq. (A3):

$$\zeta' = \xi + (1 + g' - g)\Phi_- + (g+1)\Phi'_- - \frac{V_T}{k_H} \frac{H'}{H}. \quad (A4)$$

For practical reasons, Eq. (35) is re-written in a symbolic manner as  $\Phi_- = X - \Gamma$ , so its derivative turns to be  $\Phi'_- = X' - \Gamma'$ ; a redefinition like that allows us to go through a large computation without losing clarity in the process. Replacing  $\Phi_-$  along with  $\Phi'_-$  into (A4) leads to

$$\begin{aligned} \zeta' = & \xi - (1+g)(\Gamma + \Gamma') + (g+1)(X + X') \\ & + (g' - 2g)(X - \Gamma) - \frac{V_T}{k_H} \frac{H'}{H}. \end{aligned} \quad (A5)$$



As a result, Eq. (A5) gives the final form for the source term in a very generic manner

$$S = \frac{(g' - 2g)}{(g + 1)} \Phi_- + (X + X') + \left[ \frac{\xi - \zeta' - \frac{V_T}{k_H} \frac{H'}{H}}{g + 1} \right], \quad (\text{A6})$$

where  $S \equiv \Gamma + \Gamma'$ . Using  $\frac{da^2}{d \ln a} = 2a^2$  for obtaining  $X'$  in terms of  $X$ , we can write the second term in Eq. (A5) as

$$X + X' = \frac{\kappa a^2}{2k^2} \frac{3(\Delta_T \rho_T + c_K p_T \Pi_T)}{c_K} + \frac{\kappa a^2}{2k^2} \frac{(\Delta_T \rho_T)' + c_K (p_T \Pi_T)'}{c_K}. \quad (\text{A7})$$

In what follows, we take out as a common factor  $\kappa a^2 [2(g + 1)k^2]^{-1}$  in Eq. (A6):

$$S = \frac{(g' - 2g)}{(g + 1)} \Phi_- + \frac{\kappa a^2}{2(g + 1)k^2} \left[ \frac{3(g + 1)(\Delta_T \rho_T + c_K p_T \Pi_T)}{c_K} + (g + 1) \frac{(\Delta_T \rho_T)' + c_K (p_T \Pi_T)'}{c_K} + \frac{2k^2}{\kappa a^2} \left( \xi - \zeta' - \frac{V_T}{k_H} \frac{H'}{H} \right) \right]. \quad (\text{A8})$$

We have to re-write (A8) a little bit more. For instance, the  $(\Delta_T \rho_T)'$  term is replaced by taking into account the modified continuity equation

$$\frac{(\Delta_T \rho_T)'}{c_K} = - \frac{3[\Delta_T \rho_T + \Delta p_T]}{c_K} - (\rho_T + p_T) \frac{[k_H V_T + 3\zeta']}{c_K} + \frac{\Delta Q_c - \xi Q_c}{H c_K}, \quad (\text{A9})$$

Inserting (A9), (A10), and (A14) into (A8), we find that the source term in the large scale limit ( $k_H \ll 1$ ) can be written as

$$S = \frac{(g' - 2g)}{(g + 1)} \Phi_- + \frac{\kappa a^2}{2(g + 1)k^2} \left[ (g + 1)(p_T \Pi_T + (p_T \Pi_T)') + \frac{3(g + 1)a}{k c_K} [Q_c(V - V_T) + F_c] + \frac{(g + 1)}{H c_K} [\Delta Q_c - \xi Q_c] + V_T k_H [(\rho_T + p_T)(-g - f_\zeta(g + 1)) + (\rho_e + p_e)] \right], \quad (\text{A15})$$

which implies

$$\lim_{k_H \ll 1} \Gamma' = S - \Gamma. \quad (\text{A16})$$

Some comments are in order. First, regular terms like  $k^2 V_T k_H = \mathcal{O}(\zeta k^4 / \mathcal{H}^2)$  can be dropped provided the method relies on the assumption  $V_T = \mathcal{O}(\zeta k / \mathcal{H})$ . Besides, a term like  $p_T \Pi_T + (p_T \Pi_T)'$  can be neglected in the latter expression provided  $p_T \Pi_T + (p_T \Pi_T)' = \mathcal{O}(k^2)$ ; moreover,  $\Pi_e \gg \Pi_T$ . For  $\Delta Q_c = 0$  and  $Q_c = 0$ , we recover the usual formula reported by Hu in his seminal article [89].

where the perturbation of total pressure term can be replaced by taking into account the N-S equation for total matter (excluding effective dark energy):

$$-3 \frac{\Delta p_T}{c_K} = \frac{-2c_K p_T \Pi_T + 3(\rho_T + p_T)\xi}{c_K} + 3 \frac{a}{k} \frac{[Q_c(V - V_T) + f_c]}{c_K}. \quad (\text{A10})$$

On the other hand, the last three terms in (A8) may be replaced by using (27) for obtaining

$$3(\zeta' - \xi) = - \frac{3K V_T k_H}{k^2} - \frac{3\kappa}{2H^2} [(\rho_e + p_e) \frac{V_e - V_T}{k_H}]. \quad (\text{A11})$$

Note that

$$\zeta' - \xi + \frac{V_T}{k_H} \frac{H'}{H} = \zeta' - \xi + V_T k_H \frac{H' H}{(H k_H)^2}, \quad (\text{A12})$$

while the derivative of Friedmann equation leads to

$$H H' = \frac{K}{a^2} - \frac{\kappa}{2} [(\rho_T + p_T) + (\rho_e + p_e)]. \quad (\text{A13})$$

Employing the third Einstein equation (27) and replacing (A13) into (A12), we arrive at the following expression:

$$\zeta' - \xi + \frac{V_T}{k_H} \frac{H'}{H} = - \frac{\kappa}{2H^2} (\rho_e + p_e) \frac{V_e - V_T}{k_H} - \frac{\kappa V_T k_H a^2}{2k^2} [(\rho_T + p_T) + (\rho_e + p_e)]. \quad (\text{A14})$$

## Appendix B: Writing the source term in synchronous gauge

An important issue regarding the numerical implementation of PPF method is that all physical quantities such the source term must be given in the synchronous gauge. We will discuss with enough detail the gauge transformations for going from the co-moving gauge to synchronous one because they are essentials for understanding all the modifications that the code needs.

The transformation law from comoving to synchronous gauge for matter density perturbation, including dark

matter, is

$$\Delta_T \rho_T = \delta_T^s \rho_T + 3(\rho_T + p_T)(v_T^s/k_H) - \bar{Q}_c(v_T^s/k_H), \quad (\text{B1})$$

where we used the background balance equation. For effective dark energy, we have a similar expression

$$\Delta_e \rho_e = \delta_e^s \rho_e + 3(\rho_e + p_e)(v_T^s/k_H) - \bar{Q}_e(v_T^s/k_H). \quad (\text{B2})$$

Then, using variables belonging to synchronous gauge only, the modified Poisson (35) equation can be recast

$$\begin{aligned} \Phi_- = & -\Gamma + \frac{\kappa a^2}{2c_K k^2} [\delta_T^s \rho_T + 3(\rho_T + p_T)(v_T^s/k_H) \\ & - \bar{Q}_c(v_T^s/k_H) + c_K p_T \Pi_T]. \end{aligned} \quad (\text{B3})$$

Besides, we get  $\Phi_-$  written in terms of synchronous variables provided  $\Pi_k$  is gauge invariant while pressure and density are both manifestly gauge-invariant because are not perturbed variables. Note that the function  $F(a)$  only depends on background variables, so we do not to apply any gauge transformation.

Replacing (B2) into Eq. (37), we get

$$\rho_e \delta_e^s + 3(\rho_e + p_e) \frac{v_e^s}{k_H} + c_K p_e \Pi_e - \bar{Q}_e \frac{v_T^s}{k_H} = -\frac{2k^2 c_K}{\kappa a^2} \Gamma. \quad (\text{B4})$$

The master equation for  $\Gamma$  with  $f_G = 0$  is given by

$$\Gamma' = -\Gamma + \frac{S}{(1 + \mathcal{H}^2 c_1^2 k^2)}, \quad (\text{B5})$$

where  $\Gamma' = \mathcal{H}^{-1} \Gamma$ . We left the gauge transformation of the source term for the end because we need additional steps.

The total matter velocity can be written in the synchronous gauge as (cf. Appendix C)

$$\frac{V_T}{k_H} = \frac{v_T^s}{k_H} + \eta_T + (g+1)\Phi_- - \frac{\kappa a^2}{2k^2} p_T \Pi_T. \quad (\text{B6})$$

Using (B3) we write matter velocity as

$$\begin{aligned} \frac{V_T}{k_H} = & \frac{v_T^s}{k_H} + (\eta_T - \Gamma) - \frac{\kappa a^2 p_e \Pi_e}{2k^2} - \frac{\kappa a^2}{2k^2} p_T \Pi_T \\ & + \frac{\kappa a^2}{2c_K k^2} [\delta_T^s \rho_T + 3(\rho_T + p_T)(v_T^s/k_H) \\ & - \bar{Q}_c(v_T^s/k_H) + c_K p_T \Pi_T], \end{aligned} \quad (\text{B7})$$

or

$$\begin{aligned} \frac{V_T}{k_H} = & \frac{v_T^s}{k_H} + (\eta_T - \Gamma) - \frac{\kappa a^2 p_e \Pi_e}{2k^2} + \frac{\kappa a^2}{2c_K k^2} [\delta_T^s \rho_T \\ & + 3(\rho_T + p_T)(v_T^s/k_H) - \bar{Q}_c(v_T^s/k_H)]. \end{aligned} \quad (\text{B8})$$

Another expression that should be transformed is the velocity of dark energy (45), in fact, only requires that

we use the gauge invariance of relative velocity, namely,  $V_e - V_T = v_e^s - v_T^s$  (see Appendix A):

$$\begin{aligned} v_e^s \kappa a^2 (\rho_e + p_e) = & -2\mathcal{H}k \times \frac{g+1}{F(a)} ([S_0 - \Gamma - \Gamma']) \\ & + \frac{\kappa a^2}{\mathcal{H}^2} f_\zeta (\rho_T + p_T) \frac{V_T}{k_H} + v_T^s \kappa a^2 (\rho_e + p_e). \end{aligned} \quad (\text{B9})$$

The third Einstein equation gives

$$\eta_T' c_K - \frac{K}{2k^2} h_L' = \frac{\kappa a^2}{2\mathcal{H}^2} \left[ (\rho_T + p_T) \frac{v_T^s}{k_H} + (\rho_e + p_e) \frac{v_e^s}{k_H} \right], \quad (\text{B10})$$

and the first Einstein equation reads

$$h_L' = \frac{2c_K k^2}{\mathcal{H}^2} \eta_T + \frac{2\kappa a^2}{\mathcal{H}^2} (\delta_T^s \rho_T^s + \delta_e^s \rho_e^s), \quad (\text{B11})$$

Inserting (B4) into (B11) leads

$$\begin{aligned} h_L' = & \frac{2c_K k^2}{\mathcal{H}^2} (\eta_T - \Gamma) + \frac{\kappa a^2}{\mathcal{H}^2} \left( \delta_T^s \rho_T^s + \bar{Q}_e \frac{v_T^s}{k_H} \right. \\ & \left. - c_K p_e \Pi_e - 3(\rho_e + p_e) \frac{v_e^s}{k_H} \right). \end{aligned} \quad (\text{B12})$$

On the other hand, the  $(\rho_e + p_e) \frac{v_e^s}{k_H}$ -term in the above equation can be obtained from third field equation (B10). Substituting the aforesaid term again into Eq. (B12) gives a constraint between  $h_L$  and  $\dot{\eta}_L$

$$\begin{aligned} \mathcal{H}\sigma = & k(\eta_T - \Gamma) + \frac{\kappa a^2}{2kc_K} \left( \delta_T^s \rho_T^s + \bar{Q}_e \frac{v_T^s}{k_H} \right. \\ & \left. - c_K p_e \Pi_e + 3(\rho_T + p_T) \frac{v_T^s}{k_H} \right), \end{aligned} \quad (\text{B13})$$

where have changed to conformal time variable in the derivatives and used the standard definition,  $2k^2\sigma = \dot{h}_L + 6\dot{\eta}_L$ . From (B13) we write the next term

$$\begin{aligned} (\eta_T - \Gamma) = & \mathcal{H} \frac{\sigma}{k} - \frac{\kappa a^2}{2k^2 c_K} \left( \delta_T^s \rho_T^s + \bar{Q}_e \frac{v_T^s}{k_H} \right. \\ & \left. - c_K p_e \Pi_e + 3(\rho_T + p_T) \frac{v_T^s}{k_H} \right). \end{aligned} \quad (\text{B14})$$

Having replaced (B14) in (B8), we can then obtain the next identity:

$$\frac{V_T}{k_H} = \frac{v_T^s + \sigma}{k_H}. \quad (\text{B15})$$

Finally, we have all the terms in Eq. (A15) written in the synchronous gauge; in fact, we still have to transform  $\Delta Q_c$ ,  $Q_c$ , and  $F_c$ , but this depends on the specific form of interaction. A more useful expression for  $S$  is given by

$$\begin{aligned} S_{\text{sync}} = & \frac{\kappa a^2}{2k^2} \left( \frac{3a}{kc_K} [Q_c(V - V_T) + F_c]_{\text{sync}} \right. \\ & + \frac{1}{Hc_K} [\Delta Q_c - \xi Q_c]_{\text{sync}} \\ & \left. + k_H (v_T^s + \sigma) [-(\rho_T + p_T) f_\zeta + (\rho_e + p_e)] \right). \end{aligned} \quad (\text{B16})$$

In addition, our aiming is to obtain the source term in terms of synchronous variables only by taking into account the explicit form of the interaction term mentioned in Sec. V. For the latter reason, we will show how to get the perturbed interaction in the synchronous gauge.

In the Case I, the PPF code needs as input the following expressions in the synchronous gauge:

$$\begin{aligned} [Q_c(V - V_T) + F_c]_{\text{sync}} &= [Q_c(V_c - V_T)]_{\text{sync}} \\ &= Q_c(v_c^s - v_T^s) = 0, \quad v_c^s = v_T^s, \\ [\Delta Q_c - \xi Q_c]_{\text{sync}} &= 3H\xi_c[\Delta_c\rho_c]_{\text{sync}}, \end{aligned} \quad (\text{B17})$$

where the transformation rules the perturbed densities are given by

$$[\Delta_c\rho_c]_{\text{sync}} = \delta_c^s\rho_c + 3(\rho_c + p_c)(v_T^s/k_H) - \bar{Q}_c(v_T^s/k_H). \quad (\text{B18})$$

In the case II, the PPF code needs as input the following expressions in the synchronous gauge:

$$\begin{aligned} [Q_c(V - V_T) + F_c]_{\text{sync}} &= [Q_c(V_x - V_T)]_{\text{sync}} = Q_c(v_x^s - v_T^s), \\ [\Delta Q_c - \xi Q_c]_{\text{sync}} &= 3H\xi_c[\Delta_c\rho_c]_{\text{sync}}. \end{aligned} \quad (\text{B19})$$

### Appendix C: Synchronous Gauge

We are going to outline the main ingredients for implementing the PPF prescription in terms of synchronous gauge variable only provided it is useful for writing its numerical code in fortran, as a patch of the public code dubbed CAMB [72]. We will follow the approach illustrated by Hu in [89] with some minor changes. The synchronous gauge corresponds to fix the potential and shift functions equals to zero ( $A = B = 0$ ). Replacing both conditions into gauge transformation for metric variables yields

$$\begin{aligned} \eta_T &\equiv -\frac{1}{3}H_T - H_L, \\ h_L &= 6H_L. \end{aligned} \quad (\text{C1})$$

In order to go from a synchronous gauge choice to the comoving gauge we must apply the following transformation rules

$$\begin{aligned} T &= \frac{v_T^s}{k}, \\ L &= \frac{3}{k}(\eta_T + \frac{1}{6}h_L). \end{aligned} \quad (\text{C2})$$

In the main part of the text we have been working in the comoving gauge, so it is very useful to know how to transform the comoving gauge density fluctuations in terms of its synchronous counterpart

$$\Delta_i\rho_i = \delta_i^s\rho_i - \rho_i'(v_T^s/k_H). \quad (\text{C3})$$

Eq. (26) can be used for establishing a useful link between comoving and synchronous variables

$$\zeta = -\eta_T - \frac{v_T^s}{k_H}, \quad (\text{C4})$$

while Eq. (40) leads to a relation between potential variables and anisotropic pressure fluctuations

$$\Phi = (g+1)\Phi_- - \frac{4\pi G}{H^2 k_H^2} p_T \Pi_T. \quad (\text{C5})$$

Taking into account the above two equations, we express the comoving total matter velocity variables in terms of gauge invariant quantities and variables defined in the synchronous gauge

$$\frac{V_T}{k_H} = \frac{v_T^s}{k_H} + (g+1)\Phi_- - \frac{4\pi G}{H^2 k_H^2} p_T \Pi_T + \eta_T. \quad (\text{C6})$$

The above equations turn to be useful for writing the master equation of the interpolating function (44) in the synchronous gauge.

Comoving density fluctuations can be expressed in terms of synchronous variables and background quantities as follows

$$\delta_i^s = \Delta_i + [-3(1+w_i) + \frac{\bar{Q}_i}{\rho_i}] \frac{v_T^s}{k_H}, \quad (\text{C7})$$

where  $i = x, m$ . Using the gauge invariance of relative velocity, we obtain

$$v_i^s = V_i - V_T + v_T^s. \quad (\text{C8})$$

Finally, we list the first and third Einstein equations (13) in the synchronous gauge:

$$h'_L = 2c_K k_H^2 \eta_T + \frac{8\pi G}{H^2} (\delta_T^s \rho_T^s + \delta_x^s \rho_x^s), \quad (\text{C9})$$

$$\begin{aligned} \eta'_T - \frac{3K}{k^2}(\eta'_T + \frac{1}{6}h'_L) &= \frac{4\pi G}{H^2} \left[ (\rho_T + p_T) \frac{v_T^s}{k_H} + (\rho_x + p_x) \frac{v_x^s}{k_H} \right]. \end{aligned} \quad (\text{C10})$$

### Appendix D: Dark matter perturbations

For a generic I-fluid component, the standard perturbed equations for the contrast density and velocity variables [63] are given by

$$\begin{aligned} \dot{\delta}_I + 3\mathcal{H}(c_{sI}^2 - w_I)\delta_I + 9\mathcal{H}^2(1+w_I)(c_{sI}^2 - c_{aI}^2) \frac{\theta_I}{k^2} &+ (1+w_I)\theta_I - 3(1+w_I)\psi' + (1+w_I)k^2(B - E') \\ &= \frac{a}{\rho_I}(-Q_I\delta_I + \delta Q_I) + \frac{aQ_I}{\rho_I} \left[ \phi + 3\mathcal{H}(c_{sI}^2 - c_{aI}^2) \frac{\theta_I}{k^2} \right], \\ \dot{\theta}_I + \mathcal{H}(1 - 3c_{sI}^2)\theta_I - \frac{c_{sI}^2}{(1+w_I)}k^2\delta_I - k^2\phi &= \frac{a}{(1+w_I)\rho_I}[(Q_I\theta - k^2 f_I) - (1+c_{sI}^2)Q_I\theta_I], \end{aligned} \quad (\text{D1})$$

where the overdot refers to conformal time derivative, the density contrast is defined as  $\delta_I = \delta\rho_I/\rho_I$ , and the anisotropic stress contribution is neglected,  $\pi_I = 0$ . Above,  $c_{aI}^2$  stands for the adiabatic sound speed defined as  $c_{aI}^2 = \dot{p}_I/\dot{\rho}_I = w_I + \dot{w}_I/(\dot{\rho}_I/\rho_I)$ , while  $c_{sI}^2$  is the I-fluid physical sound speed in the rest frame, namely  $c_{sI}^2 = (\delta p_I/\delta\rho_I)_{\text{rest frame}}$ . The synchronous gauge corresponds to  $\phi = B = 0$ ,  $\psi = \eta$ , and  $k^2 E = -h/2 - 3\eta$ . In the case of dark matter, we use  $w_c = c_{sc}^2 = c_{ac}^2 = 0$ . Then, the perturbations of dark matter variables lead to

$$\begin{aligned}\dot{\delta}_c + \theta_c + \frac{\dot{h}}{2} &= \frac{a}{\rho_c} [\delta Q_c - \delta_c Q_c], \\ \dot{\theta}_c + \theta_c \mathcal{H} &= \frac{a}{\rho_c} [Q_c(\theta - \theta_c) - k^2 F_c].\end{aligned}\quad (\text{D2})$$

In the case I, we have  $F_c = Q_c(V_c - V)$  or  $-k^2 F_c = Q_c(\theta_c - \theta)$ ,  $Q_c = 3H\xi_c\rho_c$ , and  $\delta Q_c = 3H\xi_c\delta\rho_c$ . Using the latter expressions, we find that  $[Q_c(\theta - \theta_c) - k^2 F_c] = 0$  and  $a[\delta Q_c - \delta_c Q_c] = 3H\xi_c[\delta_c - \delta_c]\rho_c = 0$ , and therefore

the master equations are given by

$$\begin{aligned}\dot{\delta}_c + \theta_c + \frac{\dot{h}}{2} &= 0, \\ \dot{\theta}_c + \theta_c \mathcal{H} &= 0.\end{aligned}\quad (\text{D3})$$

We recovered the case studied by Yue *et al.* previously [106].

In the case II, we have  $F_c = Q_c(V_x - V)$  or  $-k^2 F_c = Q_c(\theta_x - \theta)$ ,  $Q_c = 3H\xi_c\rho_c$ , and  $\delta Q_c = 3H\xi_c\delta\rho_c$ . Using the latter expressions, we find that  $[Q_c(\theta - \theta_c) - k^2 F_c] = [Q_c(\theta_x - \theta_c)]$  and  $a[\delta Q_c - \delta_c Q_c] = 0$ , and therefore the master equations are given by

$$\begin{aligned}\dot{\delta}_c + \theta_c + \frac{\dot{h}}{2} &= 0, \\ \dot{\theta}_c + \theta_c \mathcal{H} &= 3H\xi_c(\theta_x - \theta_c).\end{aligned}\quad (\text{D4})$$

- 
- [1] Astrophys.J.Suppl. 208 (2013) 19 arXiv:1212.5226.
  - [2] Planck 2013 results. I. Overview of products and scientific results - Planck Collaboration (Ade, P.A.R. et al.) arXiv:1303.5062.
  - [3] Planck 2013 results. XV. CMB power spectra and likelihood - Planck Collaboration (Ade, P.A.R. et al.) arXiv:1303.5075.
  - [4] Planck 2013 results. XVI. Cosmological parameters - Planck Collaboration (Ade, P.A.R. et al.) arXiv:1303.5076.
  - [5] 2dFGRS Collaboration (Percival, Will J. et al.), Mon.Not.Roy.Astron.Soc. 353 (2004) 1201, astro-ph/0406513.
  - [6] Reid, Beth A. et al. arXiv:1203.6641 [astro-ph.CO]
  - [7] Manera, Marc et al. Mon.Not.Roy.Astron.Soc. **428** (2012) 2, 1036-1054 arXiv:1203.6609.
  - [8] Beutler, Florian et al. Mon.Not.Roy.Astron.Soc. **423** (2012) 3430-3444 arXiv:1204.4725.
  - [9] Beutler, Florian et al. Mon.Not.Roy.Astron.Soc. 416 (2011) 3017-3032 arXiv:1106.3366 [astro-ph.CO]
  - [10] Padmanabhan, N., Xu, X., Eisenstein, D. J., Scalzo, R., Cuesta, A. J., Mehta, K. T., Kazin, E., arXiv:1202.0090
  - [11] Anderson, L., et al. 2012, arXiv:1203.6594.
  - [12] Blake, C., et al. 2011, MNRAS, 418, 1725; Blake, C., et al. 2012, MNRAS, 425, 405.
  - [13] de la Torre, S. et al. arXiv:1303.2622.
  - [14] Blake, Chris et al. Mon.Not.Roy.Astron.Soc. 415 (2011) 2876 arXiv:1104.2948.
  - [15] Samushia, Lado et al. Mon.Not.Roy.Astron.Soc. 420 (2012) 2102-2119 arXiv:1102.1014; Samushia, Lado et al. Mon.Not.Roy.Astron.Soc. 429 (2013) 1514-1528 arXiv:1206.5309.
  - [16] E. Macaulay, I.K. Wehus, and H.K. Eriksen, Phys.Rev.Lett **111** 161301 (2013).
  - [17] Song, Yong-Seon et al. JCAP **0910** (2009) 004 arXiv:0807.0810; Xu, Lixin Phys.Rev. D **87** (2013) 043525 arXiv:1302.2291; Xu, Lixin JCAP **1402** (2014) 048 arXiv:1312.4679;
  - [18] Xu, Lixin arXiv:1306.2683;
  - [19] Yang, Weiqiang et al. arXiv:1311.3419.
  - [20] Yang, Weiqiang et al. Phys.Rev. D **89** (2014) 043511 arXiv:1312.2769.
  - [21] Spyros Basilakos, [arXiv:1202.1637].
  - [22] Spyros Basilakos, Athina Pouri, [arXiv:1203.6724]; Athina Pouri, Spyros Basilakos, Manolis Plionis, [arXiv:1402.0964];
  - [23] Eisenstein, Daniel J. et al., Astrophys.J. **633** (2005) 560-574 astro-ph/0501171.
  - [24] Percival, Will J. et al. Mon.Not.Roy.Astron.Soc. **381** (2007) 1053-1066 arXiv:0705.3323.
  - [25] W.J. Percival and M. White. 2009. Mon.Not.Roy.Astron.Soc. **393** 297.
  - [26] Padmanabhan, Nikhil et al. Mon.Not.Roy.Astron.Soc. 427 (2012) 3, 2132-2145 arXiv:1202.0090 [astro-ph.CO]
  - [27] Guy, J. et al. Astron.Astrophys. **523** (2010) A7 arXiv:1010.4743; Conley, A. et al., Astrophys.J.Suppl. **192** (2011) 1, arXiv:1104.1443.
  - [28] R. Amanullah et al., Astrophys. J. **716** 712 (2010); N. Suzuki, D. Rubin and C. Lidman et al., Astrophys. J. **746**, 85 (2012).
  - [29] A. G. Riess et al. (Supernova Search Team), Astronomical Journal 116, 100938, (1998); A. G. Riess et al., Astrophysical Journal 607 665 (2004); S. Perlmutter et al. (The Supernova Cosmology Project), Astrophysical J. 517 56586, (1999); S. Perlmutter et. al., Nature 391 51 (1998).
  - [30] SNLS Collaboration, Sullivan, M. et al. Astrophys.J. **737** (2011) 102 arXiv:1104.1444; Kessler, Richard et al. Astrophys.J.Suppl. **185** (2009) 32-84 arXiv:0908.4274.
  - [31] Betoule M et al 2014 arXiv:1401.4064 Coincidence problem Concidence-issue (also CCP)
  - [32] Ivaylo Zlatev, Limin Wang, Paul J. Steinhardt, Phys. Rev. Lett. **82**, 896 (1999).
  - [33] Phenomenology of the Invisible Universe - Peebles, P.J.E. AIP Conf.Proc. 1241 (2010) 175-182 arXiv:0910.5142.

- [34] Zimdahl, Winfried et al. Phys.Lett. B **521** (2001) 133-138.
- [35] Chimento, Luis P. et al. Phys.Rev. D **67** (2003) 083513.
- [36] Huey, Greg et al. Phys.Rev. D **74** (2006) 023519 astro-ph/0407196 Sadjadi, H.Mohseni et al. Phys.Rev. D **74** (2006) 103007. Barrow, John D. et al. Phys.Rev. D **73** (2006) 103520. Lip, Sean Z.W. Phys.Rev. D **83** (2011) 023528
- [37] Sergio del Campo, Ramon Herrera, German Olivares, Diego Pavón, Phys.Rev. D **74** (2006) 023501.
- [38] Sergio del Campo, Ramon Herrera, Diego Pavón, JCAP **0901** (2009) 020. Sergio del Campo, Ramon Herrera, Diego Pavon, Phys.Rev. D **78** (2008) 021302. Diego Pavon, Winfried Zimdahl, Phys.Lett. B **628** (2005) 206-210.
- [39] Amendola, Luca et al. Phys.Rev. D **74** (2006) 023525 astro-ph/0605488.
- [40] Tocchini-Valentini, Domenico et al. Phys.Rev. D **65** (2002) 063508 astro-ph/0108143.
- [41] Amendola, Luca Phys.Rev. D **60** (1999) 043501 astro-ph/9904120.
- [42] Wetterich, Christof Astron.Astrophys. **301** (1995) 321-328 hep-th/9408025.
- [43] Holden, Damien J. et al. Phys.Rev. D **61** (2000) 043506 gr-qc/9908026.
- [44] Das, Subinoy et al. Phys.Rev. D **73** (2006) 083509 astro-ph/0510628.
- [45] Hwang, Jai-chan et al. Phys.Rev. D **64** (2001) 103509 astro-ph/0108197
- [46] Amendola, Luca Phys.Rev. D **69** (2004) 103524, astro-ph/0311175; Amendola, Luca Phys.Rev. D **62** (2000) 043511, astro-ph/9908023; Amendola, Luca Mon.Not.Roy.Astron.Soc. **312** (2000) 521, astro-ph/9906073;
- [47] Federico Marulli, Marco Baldi, Lauro Moscardini, Mon.Not.Roy.Astron.Soc. **420** (2012) 2377.
- [48] Baldi, Marco et al. JCAP **1202** (2012) 014 arXiv:1111.3953 [astro-ph.CO]. Baldi, Marco Mon.Not.Roy.Astron.Soc. **414** (2011) 116 arXiv:1012.0002.
- [49] Baldi, Marco et al. Mon.Not.Roy.Astron.Soc. **409** (2010) 89 arXiv:1007.3736.
- [50] Beynon, Emma et al. Mon.Not.Roy.Astron.Soc. **422** (2012) 3546-3553, arXiv:1111.6974.
- [51] Lee, Jounghun et al. Astrophys.J. **747** (2012) 45 arXiv:1110.0015 [astro-ph.CO].
- [52] Cui, Weiguang et al. arXiv:1201.3568; Mota, David F. JCAP **0809** (2008) 006 arXiv:0812.4493.
- [53] Manera, Marc et al. Mon.Not.Roy.Astron.Soc. **371** (2006) 1373 astro-ph/0504519.
- [54] Tarrant, Ewan R.M. et al. Phys.Rev. D **85** (2012) 023503 arXiv:1103.0694.
- [55] Tarrant, Ewan R.M. et al. Phys.Rev. D **85** (2012) 023503 arXiv:1103.0694.
- [56] Xia, Jun-Qing Phys.Rev. D **80** (2009) 103514 .
- [57] Xia, Jun-Qing JCAP **1311** (2013) 022 arXiv:1311.2131.
- [58] Ziaepour, Houry Phys.Rev. D **86** (2012) 043503 arXiv:1112.6025
- [59] Salvatelli, Valentina et al. Phys.Rev. D **88** (2013) 2, 023531 arXiv:1304.7119.
- [60] Guo, Zong-Kuan et al. Phys.Rev. D **76** (2007) 023508, astro-ph/0702015; Qiang Wu, Yungui Gong, Anzhong Wang, J.S. Alcaniz, Phys.Lett. B **659** (2008) 34-39; Abdalla, Elcio et al. Phys.Rev. D **82** (2010) 023508 arXiv:0910.5236; Cao, Shuo et al. arXiv:1012.4879. Caldera-Cabral, Gabriela et al. Phys.Rev. D **79** (2009) 063518 arXiv:0812.1827. Boehmer, Christian G. et al. Phys.Rev. D **81** (2010) 083003 arXiv:0911.3089; Boehmer, Christian G. et al. Phys.Rev. D **78** (2008) 023505 arXiv:0801.1565; Fu, Tian-Fu et al. Eur.Phys.J. C **72** (2012) 1932 arXiv:1112.2350; Li, Yun-He et al. Eur.Phys.J. C **71** (2011) 1700 arXiv:1103.3185; Chen, Xi-ming et al. JCAP **0904** (2009) 001 arXiv:0812.1117; Bolotin, Yu. L. et al. arXiv:1310.0085; Tong, M.L. et al. Class.Quant.Grav. **28** (2011) 055006 arXiv:1101.5199. Aviles, Alejandro et al. Phys.Rev. D **84** (2011) 083515, Erratum-ibid. D **84** (2011) 089905, arXiv:1108.2457. De Bernardis, Francesco et al. Phys.Rev. D **84** (2011) 023504 arXiv:1104.0652; G. Kremer, Gen.Rel.Grav. **39**, 965-972 (2007); L. P. Chimento et al Gen.Rel.Grav. **41** (2009) 1125-1137.
- [61] He, Jian-Hua et al. JCAP **0806** (2008) 010 arXiv:0801.4233; He, Jian-Hua et al. Phys.Rev. D **83** (2011) 063515 arXiv:1012.3904; Zhang, Ming-Jian et al. arXiv:1312.0224. Costa, Andr A. et al. arXiv:1311.7380.
- [62] Abdalla, E. et al. Phys.Lett. B **673** (2009) 107-110 arXiv:0710.1198 [astro-ph]
- [63] Yang, Weiqiang et al. arXiv:1401.5177.
- [64] Chimento, Luis P. et al. Phys.Rev. D **88** (2013) 087301; Chimento, Luis P. et al. Phys.Rev. D **85** (2012) 127301; Chimento, Luis P. et al. arXiv:1207.1492 [astro-ph.CO]; Chimento, Luis P. et al. Phys.Rev. D **84** (2011) 123507.
- [65] E. Calabrese, D. Huterer, E. V. Linder, A. Melchiorri and L.Pagano, Phys.Rev.D **83** 123504 (2011).
- [66] E. Calabrese, R. de Putter, D. Huterer, E. V. Linder, A. Melchiorri, Phys.Rev.D **83** 023011 (2011).
- [67] H. Kodama and M. Sasaki. 1984. Prog.Theor.Phys.,**78**,1.
- [68] Ma, Chung-Pei et al. Astrophys.J. **455** (1995) 7-25 astro-ph/9506072.
- [69] Hu, Wayne Astrophys.J. **506** (1998) 485-494 astro-ph/9801234; Hu, Wayne T, astro-ph/9508126 ; Gordon, Christopher et al. Phys.Rev. D **70** (2004) 083003, astro-ph/0406496.
- [70] Hwang, Jai-chan et al. Class.Quant.Grav. **19** (2002) 527-550, astro-ph/0103244.
- [71] William J. Potter and Sirichai Chongchitnan, JCAP **1109** (2011) 005 arXiv:1108.4414.
- [72] Lewis, Antony et al. Astrophys.J. **538** (2000) 473-476. astro-ph/9911177, <http://camb.info/>.
- [73] Lewis, Antony et al. Phys.Rev. D **66** (2002) 103511. astro-ph/0205436, <http://cosmologist.info/cosmomc/>.
- [74] Bean, Rachel et al. Phys.Rev. D **78** (2008) 023009, arXiv:0709.1128.
- [75] Bean, Rachel et al. New J.Phys. **10** (2008) 033006, arXiv:0709.1124.
- [76] Corasaniti, Pier Stefano Phys.Rev. D **78** (2008) 083538, arXiv:0808.1646.
- [77] Chongchitnan, Sirichai Phys.Rev. D **79** (2009) 043522, arXiv:0810.5411.
- [78] Valiviita, Jussi et al. JCAP **0807** (2008) 020, arXiv:0804.0232.
- [79] Gavela, M.B. et al. JCAP **0907** (2009) 034, Erratum-ibid. **1005** (2010), arXiv:0901.1611.
- [80] On the large-scale instability in interacting dark energy and dark matter fluids - Jackson, Brendan M. et al. Phys.Rev. D **79** (2009) 043526, arXiv:0901.3272.

- [81] Majerotto, Elisabetta et al. Mon.Not.Roy.Astron.Soc. **402** (2010) 2344-2354, arXiv:0907.4981.
- [82] Valiviita, Jussi et al. Mon.Not.Roy.Astron.Soc. **402** (2010) 2355-2368, arXiv:0907.4987.
- [83] Clemson, Timothy et al. Phys.Rev. D **85** (2012) 043007, arXiv:1109.6234.
- [84] Koshelev, N.A. Gen.Rel.Grav. **43** (2011) 1309-1321, arXiv:0912.0120.
- [85] Sun, Cheng-Yi et al. JCAP **1308** (2013) 018, arXiv:1303.0684.
- [86] Li, Yun-He et al. arXiv:1312.6328.
- [87] L.P.Chimento, Phys.Rev.D **81** 043525 (2010).
- [88] W.Hu and I. Sawicki, Phys.Rev. D **76** (2007) 104043.
- [89] W.Hu, Phys.Rev.D**77** 103524 (2008).
- [90] Wenjuan Fang, Sheng Wang , Wayne Hu , Zoltan Haiman, Lam Hui , Morgan May, Phys.Rev. D **78** (2008) 103509
- [91] Wenjuan Fang, Wayne Hu , Antony Lewis, Phys.Rev. D **78** (2008) 087303.
- [92] Lucas Lombriser , Anze Slosar , Uros Seljak , Wayne Hu, Phys.Rev. D **85** (2012) 124038.
- [93] Bin Hu, Michele Liguori, Nicola Bartolo, Sabino Matarrese, Phys.Rev. D **88** (2013) 2, 024012.
- [94] Lucas Lombriser, Jaiyul Yoo, Kazuya Koyama. Phys.Rev. D **87** (2013) 104019.
- [95] Scott F. Daniel, Robert R. Caldwell , Asantha Cooray, Alessandro Melchiorri , Phys.Rev. D **77** (2008) 103513; Scott F. Daniel, Robert R. Caldwell, Asantha Cooray, Paolo Serra, Alessandro Melchiorri, Asantha Cooray, Paolo Serra, Alessandro Melchiorri, Phys.Rev. D **80** (2009) 023532; Scott F. Daniel, Phys.Rev. D**80** (2009) 083520; Scott F. Daniel , Eric V. Linder , Tristan L. Smith , Robert R. Caldwell , Asantha Cooray, Alexie Leauthaud, Lucas Lombriser, Phys.Rev. D**81** (2010) 123508.
- [96] M. Bañados, P.G. Ferreira, C. Skordis, Phys.Rev. D**79** (2009) 063511
- [97] Constantinos Skordis, Phys.Rev. D**79** (2009) 123527.
- [98] Pedro G. Ferreira, Constantinos Skordis, Phys.Rev. D **81** (2010) 104020.
- [99] Jai-chan Hwang, Hyerim Noh, Chan-Gyung Park, e-Print: arXiv:1012.0885.
- [100] Richard A. Battye, Jonathan A. Pearson, JCAP **1207** (2012) 019.
- [101] Daniele Bertacca , Nicola Bartolo, Sabino Matarrese, JCAP **1208** (2012) 021.
- [102] Jason N. Dossett, Mustapha Ishak, Jacob Moldenhauer, Phys.Rev. D **84** (2011) 123001.
- [103] Gong-Bo Zhao, Levon Pogorian, Alessandra Silvestri, Joel Zylberberg, Phys.Rev. D**79** (2009) 083513. test MG.
- [104] Alireza Hojjati, Levon Pogorian , Gong-Bo Zhao, JCAP **1108** (2011) 005
- [105] Jian-hua He, Phys.Rev. D **86** (2012) 103505.
- [106] Yun-He Li, Jing-Fei Zhang, Xin Zhang, arXiv:1404.5220.
- [107] Y. Wang, D. Wands, G.B. Zhao, L. Xu, arXiv:1404.5706.
- [108] A. G. Riess, et al., ApJ **730** 119 (2011).